

Electronic Supplementary Information for

Metastable Zr/Hf-MOFs: the hexagonal family of EHU-30 and their water-sorption induced structural transformation

Maite Perfecto-Irigaray,^a Garikoitz Beobide,^{*a,b} Sofia Calero,^{c,d} Oscar Castillo,^{*a,b} Ivan da Silva,^e Juan José Gutiérrez-Sevillano,^d Antonio Luque,^{a,b} Sonia Pérez-Yáñez^{a,b,f} and Leticia F. Velasco^g

^a Departamento de Química Orgánica e Inorgánica, Facultad de Ciencia y Tecnología, Universidad del País Vasco/Euskal Herriko Unibertsitatea, UPV/EHU, Apartado 644, E-48080 Bilbao, Spain.

^b BCMaterials, Basque Center for Materials, Applications and Nanostructures, UPV/EHU Science Park, 48940 Leioa, Spain.

^c Materials Simulation & Modeling, Department of Applied Physics, Eindhoven University of Technology, 5600 MB Eindhoven, The Netherlands.

^d Department of Physical, Chemical and Natural Systems, Universidad Pablo de Olavide, Ctra. Utrera Km. 1, 41013 Seville, Spain.

^e ISIS Facility, STFC Rutherford Appleton Laboratory, Chilton, Oxfordshire OX11 0QX, U.K.

^f Departamento de Química Inorgánica, Facultad de Farmacia, Universidad del País Vasco/Euskal Herriko Unibertsitatea, UPV/EHU, E-01006 Vitoria-Gasteiz, Spain.

^g Department of Chemistry, Royal Military Academy, Renaissancelaan 30, 1000 Brussels, Belgium.

S0. PHYSICAL MEASUREMENTS	2
S1. SYNTHESIS OF EHU-30-NH ₂ AND EHU-30-NHR	4
S2. FOURIER-TRANSFORM INFRARED SPECTRA (FTIR) OF EHU-30-NH ₂ AND EHU-30-NHR	7
S3. NUCLEAR MAGNETIC RESONANCE (NMR) SPECTROSCOPY OF EHU-30-NH ₂ AND EHU-30-NHR	9
S4. THERMOGRAVIMETRIC ANALYSIS OF EHU-30-NH ₂ AND EHU-30-NHR	13
S5. POWDER X-RAY THERMODIFFRACTION (TDX) OF EHU-30-NH ₂ AND EHU-30-NHR	17
S6. TEM AND SEM MICROGRAPHS OF EHU-30-NH ₂ AND EHU-30-NHR	21
S7. CRYSTAL STRUCTURE ELUCIDATION	25
S8. COMPUTATIONAL DETAILS	30
S9. GAS ADSORPTION DATA	37
S10. WATER-VAPOUR ADSORPTION OF EHU-30(ZR), EHU-30-NH ₂ (ZR) AND EHU-30-NHR(ZR)	42
S11. LOCATION OF WATER MOLECULES BY TOF NEUTRON POWDER DIFFRACTION	48

S0. PHYSICAL MEASUREMENTS

SO. PHYSICAL MEASUREMENTS

Routine powder X-ray diffraction (PXRD) measurements were performed on a Phillips X'PERT diffractometer (equipped with Cu-K α radiation, $\lambda = 1.5418 \text{ \AA}$) over the 5–70° 2 θ range with a step size of 0.02°, a variable automatic divergence slit and an acquisition time of 2.5 s per step, at 20 °C.

High resolution XRD data were collected on a Bruker D8 Advance diffractometer equipped with a Cu tube, Ge(111) incident beam monochromator (equipped with Cu-K α_1 radiation, $\lambda = 1.5406 \text{ \AA}$) and 1-D LynxEye detector (active length in 2 θ 2.7°). Samples were mounted on zero background silicon wafers embedded in generic sample holders. Data were collected from 5 to 80° 2 θ (step size 0.02° and time per step = 20 s) at 20 °C. Fixed divergence and anti-scatter slits of 1°, giving a constant volume of sample illumination, were used.

Variable temperature PXRD data were collected on a Bruker D8 Advance diffractometer operating at 30 kV and 20 mA, equipped with a Cu tube (equipped with Cu-K α radiation, $\lambda = 1.5418 \text{ \AA}$), a Vantec-1 PSD detector, and an Anton Parr HTK2000 high-temperature furnace. The powder patterns were recorded in the 5–38° 2 θ range using steps of 0.033° and 1 s per step. Data sets were recorded in air atmosphere each 10 °C from 30 to 500 °C, using a heating rate of 0.166 °C·s $^{-1}$.

Fourier-transform infrared (FTIR) spectra of the samples (KBr pellet) were recorded at a resolution of 4 cm $^{-1}$ in the 4000–400 cm $^{-1}$ region using a FTIR 8400S Shimadzu spectrometer.

Thermal analysis (TGA) was performed on a METTLER TOLEDO TGA/SDTA851 thermal analyser in synthetic air (80% N $_2$, 20% O $_2$) flux of 50 cm 3 ·min $^{-1}$, from room temperature to 800 °C with heating rate of 5 °C min $^{-1}$ and a sample size of about 10–20 mg per run.

Transmission electron microscopy (TEM) studies were done on a TECNAI G2 20 TWIN operated at 200 kV and equipped with LaB $_6$ filament. The samples for TEM were prepared by dispersion into ethanol solvent and keeping the suspension in an ultrasonic bath for 15 min, later a drop of suspension was spread onto a TEM copper grid (300 Mesh) covered by a holey carbon film followed by drying under vacuum.

$^1\text{H-NMR}$ spectra were acquired in a Bruker AVANCE 500 (one-bay; 500 MHz) at 293 K. Previously to measure samples were digested in 2 mL of a 1 M NaOH solution (in deuterated water, D $_2$ O). The digestion was prolonged for 24 h, after which the solid residue corresponding to ZrO $_2$ or HfO $_2$ was filtered off and the NMR spectrum was taken on the liquid fraction.

$^{13}\text{C CPMAS NMR}$ spectra were recorded on a Bruker AVANCE III, 9.4 T system equipped with a 4 mm MAS DVT Double Resonance HX MAS probe. Larmor frequencies were 400.17 MHz and 100.63 MHz for ^1H and ^{13}C nuclei, respectively. Chemical shifts were calibrated indirectly with glycine, carbonyl peak at 176 ppm. Sample rotation frequency was 10 kHz and relaxation delay was 5 s. The number of scans was 12240. Polarization transfer was achieved with RAMP cross-polarization (ramp on the proton channel) with a contact time of 5 ms. High-power SPINAL 64 heteronuclear proton decoupling was applied during acquisition.

S1. SYNTHESIS OF EHU-30-NH₂ AND EHU-30-NHR

S1. SYNTHESIS OF EHU-30-NH₂ AND EHU-30-NHR

Synthesis of EHU-30-NH₂(Zr): Zirconium(IV) propoxide (Sigma-Aldrich, 70% wt in 1-propanol; 1.0529 g, 2.25 mmol) was mixed under continuous stirring with **isobutyric acid** (Sigma-Aldrich, 99%, 0.950 g·cm⁻³; 1400 μL, 15 mmol) and 2-aminobenzene-1,4-dicarboxylic acid (Sigma-Aldrich, 99%, 0.4117 g, 2.25 mmol) in a closed teflon vessel. Thereafter, water was added to obtain the most crystalline sample (10 μL, 0.56 mmol). The resulting reaction mixture was placed in a preheated oven at 140°C for 4 hours. The synthesis product was washed three times with methanol and dried under vacuum.

Synthesis of EHU-30-NH₂(Hf): Hafnium(IV) isopropoxide (Sigma-Aldrich, 99.9%; 0.9343 g, 2.25 mmol) was mixed under continuous stirring with **isobutyric acid** (Sigma-Aldrich, 99%, 0.950 g·cm⁻³; 1400 μL, 15 mmol) and 2-aminobenzene-1,4-dicarboxylic acid (Sigma-Aldrich, 99%, 0.4117 g, 2.25 mmol) in a closed teflon vessel. The resulting reaction mixture was placed in a preheated oven at 140°C for 4 hours. The synthesis product was washed three times with methanol and dried under vacuum.

Synthesis of EHU-30-NHR(Zr): Zirconium(IV) propoxide (Sigma-Aldrich, 70% wt in 1-propanol; 1.0529 g, 2.25 mmol) was mixed under continuous stirring with **methacrylic acid** (Sigma-Aldrich, 99%, 1.015 g·cm⁻³; 1400 μL, 16 mmol) and 2-aminobenzene-1,4-dicarboxylic acid (Sigma-Aldrich, 99%, 0.4117 g, 2.25 mmol) in a closed teflon vessel. Thereafter, water was added to obtain the most crystalline sample (50 μL, 2.78 mmol). The resulting reaction mixture was placed in a preheated oven at 140°C for 4 hours. The synthesis product was washed three times with methanol and dried under vacuum.

Synthesis of EHU-30-NHR(Hf): Hafnium(IV) isopropoxide (Sigma-Aldrich, 99.9%; 0.9343 g, 2.25 mmol) was mixed under continuous stirring with **methacrylic acid** (Sigma-Aldrich, 99%, 1.015 g·cm⁻³; 1400 μL, 16 mmol) and 2-aminobenzene-1,4-dicarboxylic acid (Sigma-Aldrich, 99%, 0.4117 g, 2.25 mmol) in a closed teflon vessel. Thereafter, water was added to obtain the most crystalline sample (20 μL, 1.11 mmol). The resulting reaction mixture was placed in a preheated oven at 140°C for 4 hours. The synthesis product was washed three times with methanol and dried under vacuum.

Structure-directing capability of modulators:

The influence of using templates with slight topological and size differences by **replacing isobutyric acid by butyric acid, propionic acid and acetic acid** in the synthesis of **EHU-30-NH₂** was studied. In all cases, the target phase was obtained but the powder X-ray diffraction (PXRD) patterns revealed an overall lowering of the crystallinity and the presence of UiO-66 as impurity (Figure S1.1). Two main principles peaks of parent EHU-30 are observed in every samples, (1 0 0) and (1 0 2), but some impurities that correspond to UiO-66 are also observed as emerging peaks (marked with asterisks and reference in the image) when using acetic acid, propionic acid and butyric acid as modulators. Full width at half maximum (FWHM) of peak (1 0 0) of EHU-30-NH₂ is established in the samples where it is possible to calculate.

The influence of water presence during the synthesis process was also studied. Water (source of hydroxide/oxide anions) is required for the formation of the zirconium/hafnium cluster, as it has been previously described.^{1,2} It can be added intentionally but it can also arise from ambient humidity or from a side reaction involving the partial esterification of carboxylic acids with the alcoxide/alcohol groups contained in Zr(IV)/Hf(IV) reagents, as it was previously demonstrated.³ Regarding the synthesis of EHU-30-NH₂ and EHU-30-NHR, in general terms, we observed that addition of water ranging stoichiometric amounts (up to 1-2 mmol of H₂O per metal ion mmol) is beneficial as it improves the crystallinity and purity of the samples. However, greater amounts of water give rise to the formation of UiO-66-NH₂/NHR impurities together with EHU-30-NH₂/NHR (Figure S1.2). Thus, it seems that the excess of water interferes with the modulator, inhibiting its ability to template the growth of the target framework, and allowing consequently, the formation of the thermodynamically favoured coordination structure, UiO-66 polymorph. The optimum amount of water is different depending on the modulator and on the metal ion employed, as can be observed in the synthesis procedures detailed above.

¹ M. Taddei, J. A. van Bokhoven and M. Ranocchiari, Influence of Water in the Synthesis of the Zirconium-Based Metal–Organic Framework UiO-66: Isolation and Reactivity of [ZrCl(OH)₂(DMF)₂]Cl, *Inorg. Chem.*, 2020, **59**, 7860–7868. <https://doi.org/10.1021/acs.inorgchem.0c00991>.

² V. V. Butova, A. P. Budnyk, K. M. Charykov, K. S. Vetlitsyna-Novikova, C. Lamberti and A. V. Soldatov, Water as a Structure-Driving Agent between the UiO-66 and MIL-140A Metal–Organic Frameworks, *Chem. Commun.*, 2019, **55**, 901–904. <https://doi.org/10.1039/C8CC07709F>.

³ M. Perfecto-Irigaray, G. Beobide, O. Castillo, I. Da Silva, D. García-Lojo, A. Luque, A. Mendia and S. Pérez-Yáñez, [Zr₆O₄(OH)₄(Benzene-1,4-Dicarboxylato)₆]_n: A Hexagonal Polymorph of UiO-66, *Chem. Commun.*, 2019, **55**, 5954–5957. <https://doi.org/10.1039/c9cc00802k>.

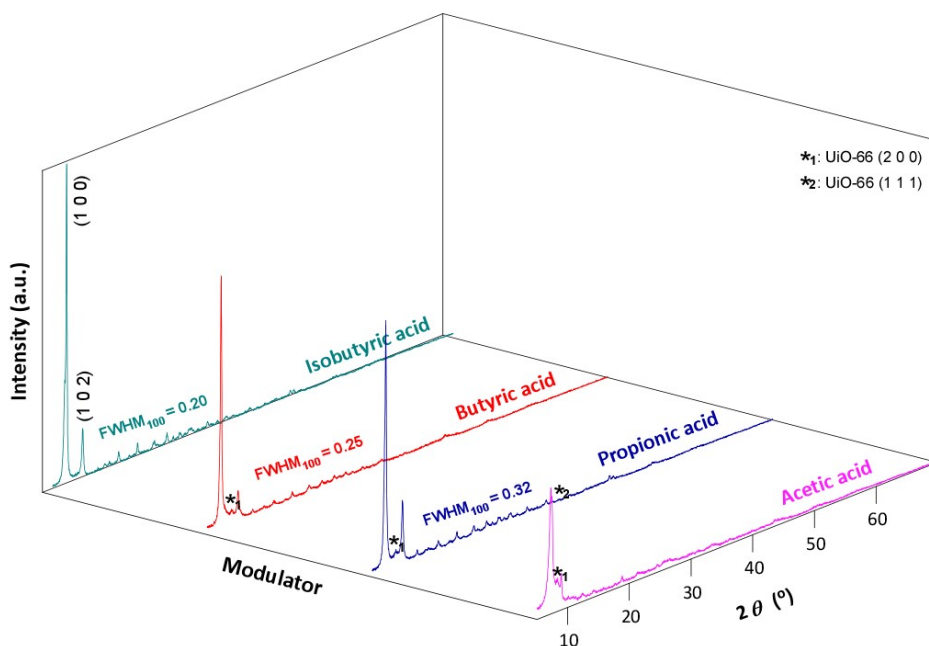


Figure S1.1. Experimental PXR D patterns for EHU-30-NH₂(Zr) samples synthesised varying the modulator (*i.e.* monocarboxylic acid). Isobutyric acid resulted the best option to obtain EHU-30-NH₂ phases.

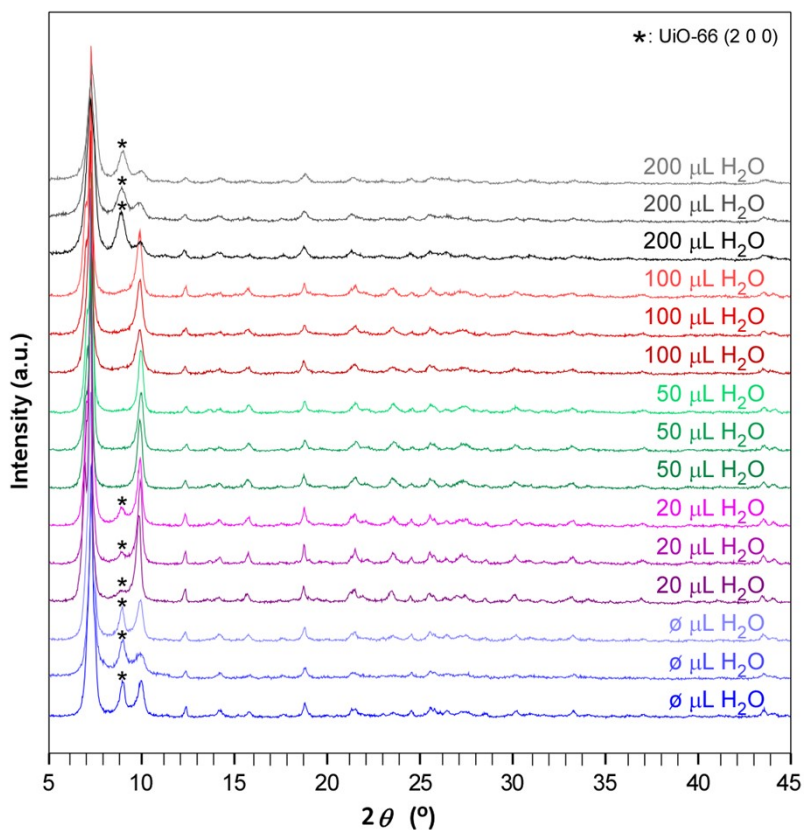


Figure S1.2. PXR D patterns of the samples resulting from the optimization process of water amount in the synthesis of EHU-30-NHR(Zr). Done in triplicate for each amount of added water.

S2. FOURIER-TRANSFORM INFRARED SPECTRA (FTIR) OF EHU-30-NH₂ AND EHU-30-NHR

S2. FOURIER-TRANSFORM INFRARED SPECTRA (FTIR) OF EHU-30-NH₂ AND EHU-30-NHR

The infrared spectra of EHU-30-NH₂ and EHU-30-NHR phases (Zr and Hf-based) and the assignment of the vibration modes are gathered in Figure S2.1. The large O–H peaks in the IR spectra is indicative of H₂O/OH⁻ pairs replacing missing linkers in the structure (see below further details in thermogravimetric analysis).

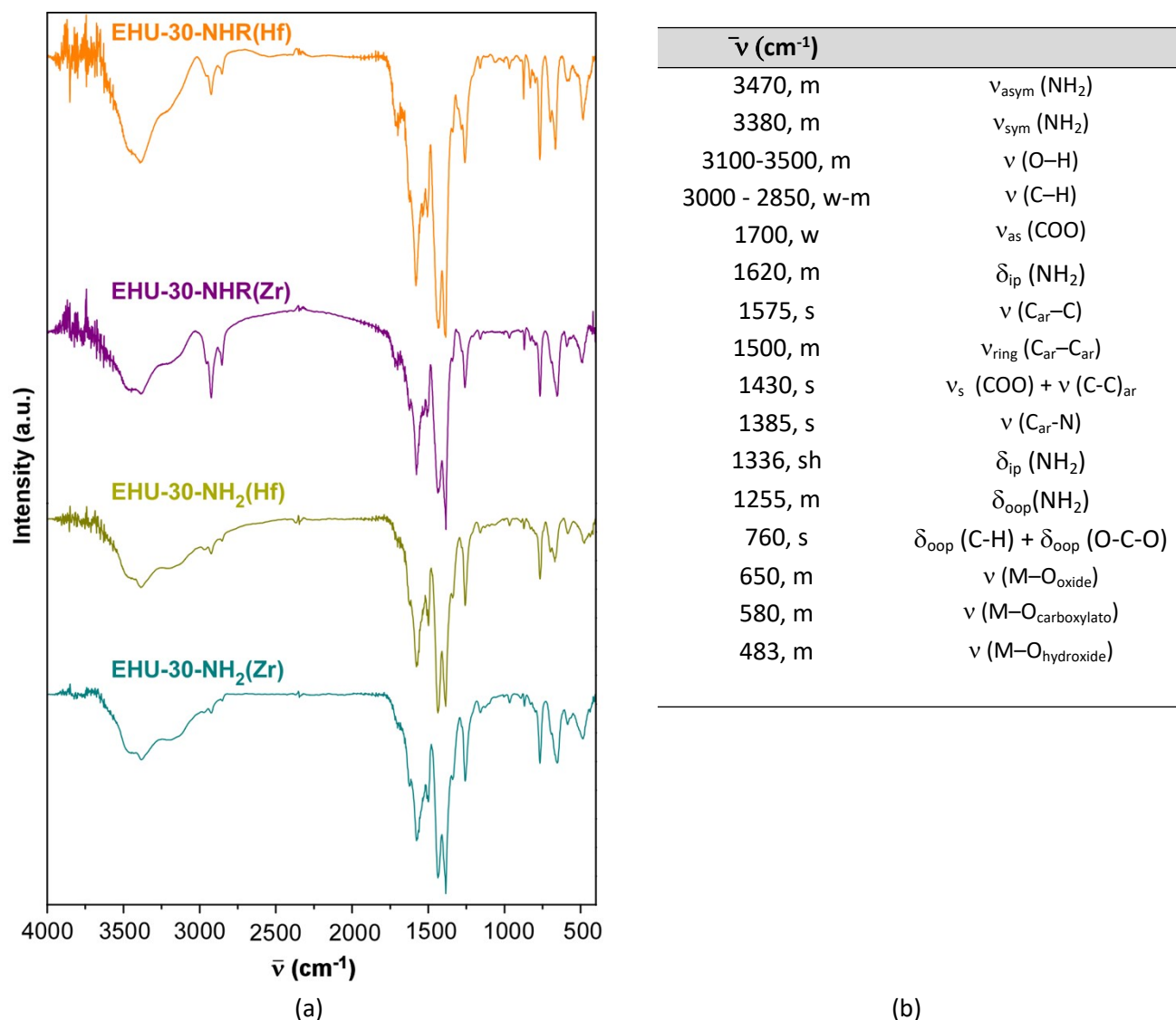


Figure S2.1. (a) FTIR spectra and (b) band assignments for EHU-30-NH₂ and EHU-30-NHR phases (s: strong, m: medium, w: weak and sh: shoulder signals; *sym* = symmetric, *asym* = asymmetric, *ip* = in plane, *ring* = ring stretching, *ar* = aromatic, *oop* = out of plane of stretchings (ν) or bendings (δ) modes).

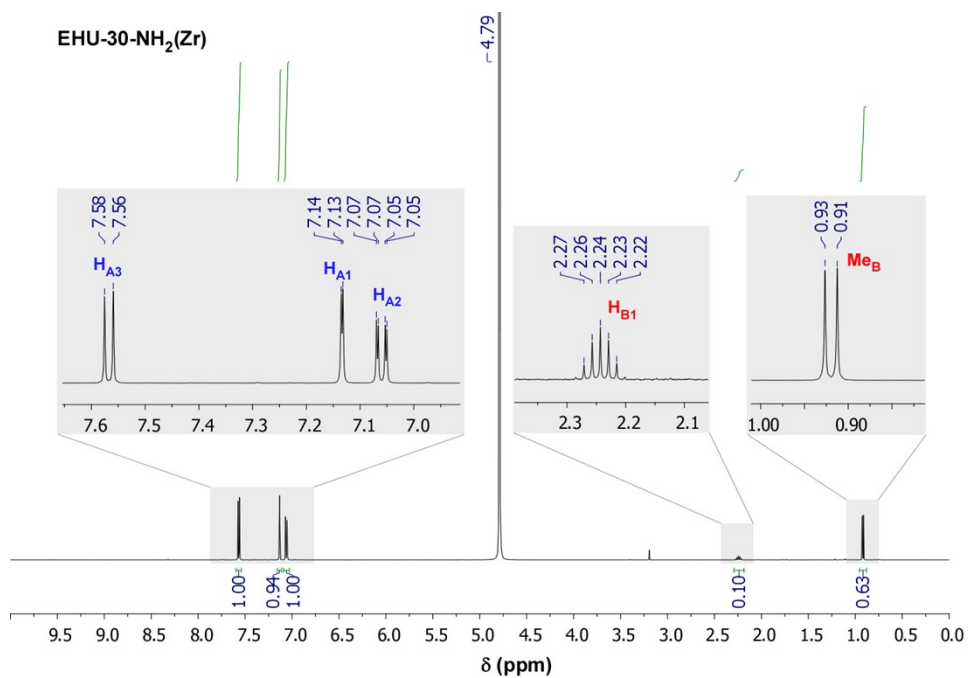
S3. NUCLEAR MAGNETIC RESONANCE (NMR) SPECTROSCOPY OF EHU-30-NH₂ AND EHU-30-NHR

S3. NUCLEAR MAGNETIC RESONANCE (NMR) SPECTROSCOPY OF EHU-30-NH₂ AND EHU-30-NHR

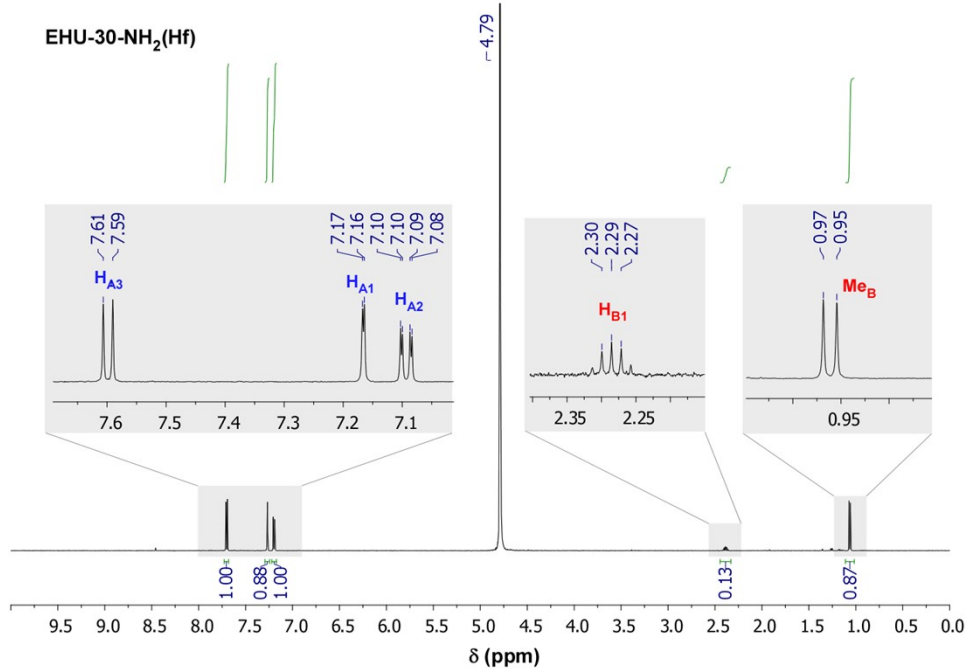
To proceed with the ¹H-NMR spectrum (500 MHz), 70 mg of each sample of EHU-30-NH₂ and EHU-30-NHR (Zr and Hf-based) was digested in 2 mL of a 1 M NaOH solution (in deuterated water, D₂O). The digestion was prolonged for 24 h, after which the solid residue corresponding to ZrO₂ or HfO₂ was filtered off and the NMR spectrum was taken on the liquid fraction (Figure S3.1 **(a)** for EHU-30-NH₂(Zr), **(b)** for EHU-30-NH₂(Hf) and Figure S3.2 **(a)** for EHU-30-NHR(Zr) and **(b)** EHU-30-NHR(Hf) with the label assignment of organic compounds present in **(c)** of each figure). The residual signal of the solvent appears at 4.79 ppm in the four spectra, then different amount of signals are observed in the two type of compounds:

EHU-30-NH₂ (Zr and Hf-based): Three signals with different multiplicity at around 7 ppm due to the aromatic protons of 2-aminobenzene-1,4-dicarboxylic acid are observed in Figure S3.1(a) and (b). Two additional signals (a multiplet at ~2 ppm that integrates to one proton and a doublet at ~1 ppm that integrates to six protons) are observed because of the presence of a small amount of isobutyric acid, the modulator used in these synthesis. The integration of the respective signals shows that the amount of isobutyric acid after the digestion of the MOFs is of a 9% relative to all carboxylic ligands (modulator plus 2-aminobenzene-1,4-dicarboxylic acid) in EHU-30-NH₂(Zr) and of a 12% in EHU-30-NH₂(Hf), what fits fairly well to that estimated from the TGA analysis (see in the following section).

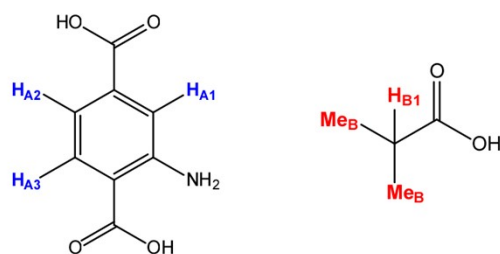
EHU-30-NHR (Zr and Hf-based): Six signals with different multiplicity at around 7 ppm due to the aromatic protons of 2-aminobenzene-1,4-dicarboxylic acid and to 2-((2-carboxypropyl)amino)benzene-1,4-dicarboxylic acid (from the Aza-Michael reaction between organic linker and methacrylic acid) are observed and assigned in Figure 3.2. The integration relation between them says that the 35% in Zr-based MOF and the 42% in Hf-based MOF of the total coordination positions occupied by a dicarboxylic ligand correspond to 2-((2-carboxypropyl)amino)benzene-1,4-dicarboxylic acid. Its presence is corroborated by the signals (three multiplets and one singlet marked in pink) observed in the 1-4 ppm range that fit fairly well with the expected positions and with the integration respect to the aromatic signals of this species in both spectra. Three additional signals (two multiplets at ~5 ppm that integrates to one proton and a doublet at ~1 ppm that integrates to six protons) are also observed because of the presence of a small amount of methacrylic acid in both digested samples. The integration of the respective signals shows that the amount of methacrylic acid after the digestion of the MOF is of a 8% relative to all carboxylic ligands (modulator plus 2-aminobenzene-1,4-dicarboxylic acid and 2-((2-carboxypropyl)amino)benzene-1,4-dicarboxylic acid) in EHU-30-NHR(Zr) and of a 11% in EHU-30-NHR(Hf), what fits also well to that estimated from the TGA analysis (see in the following section). Signals marked in green in the spectrum of Zr-based MOF digestion correspond to 1-propanol, which comes from zirconium reagent.



(a)

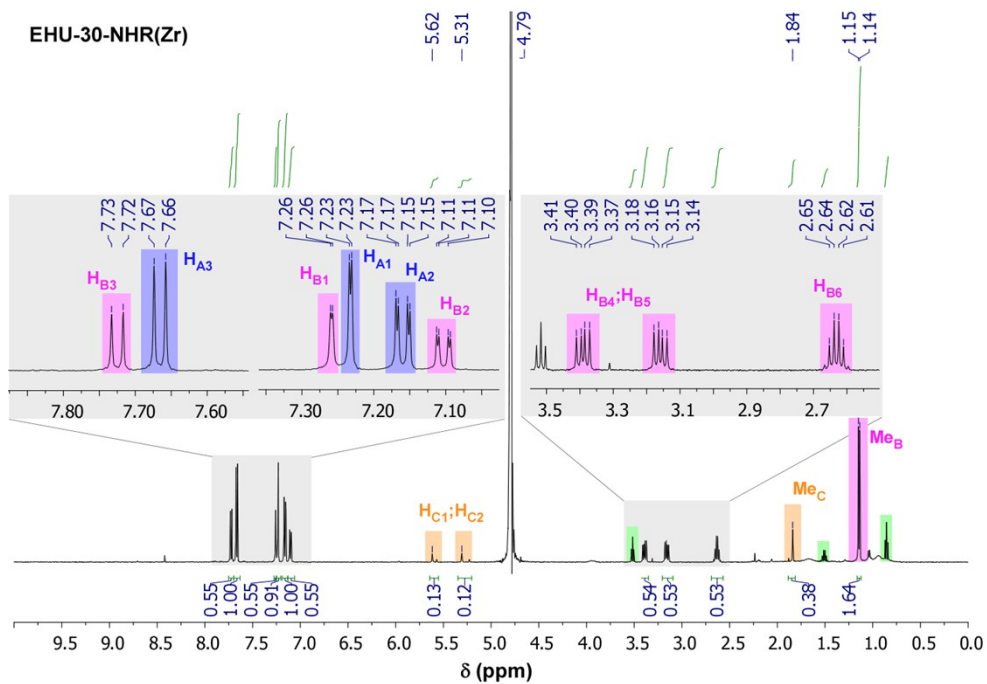


(b)

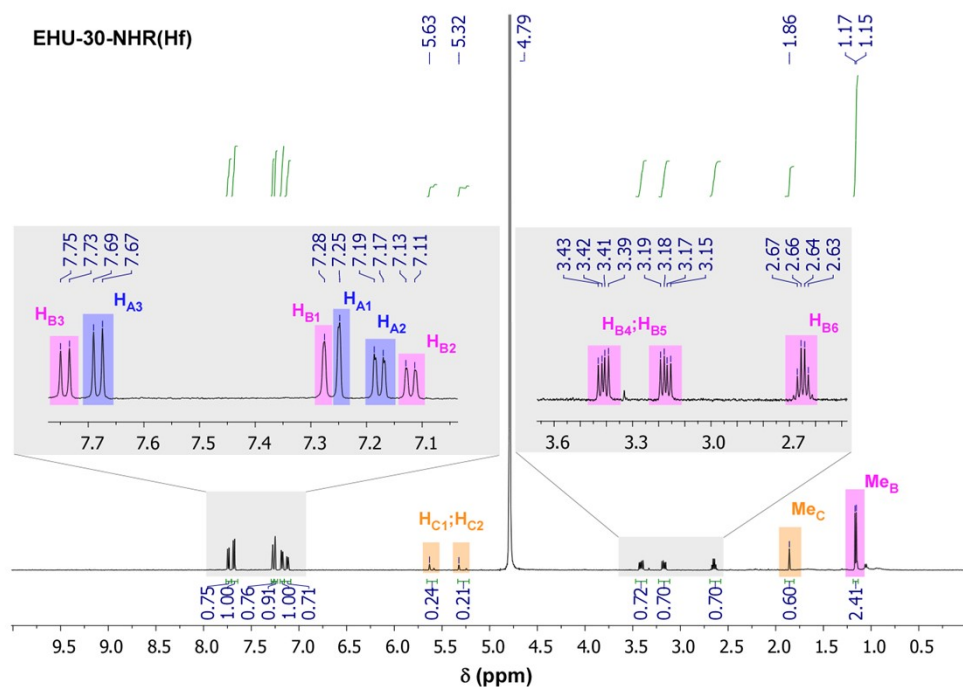


(c)

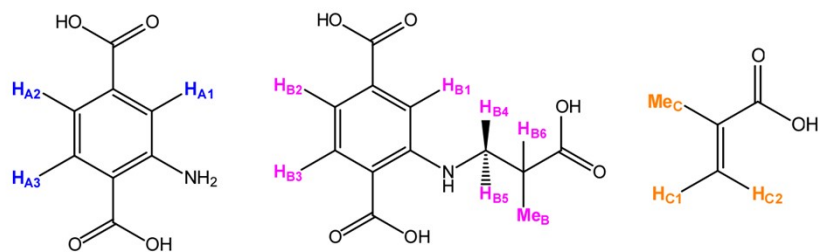
Figure S3.1. ¹H-NMR spectrum of digested (a) EHU-30-NH₂(Zr) and (b) EHU-30-NH₂(Hf). (c) Label assignment of organic compounds: 2-aminobenzene-1,4-dicarboxylic acid in blue and isobutyric acid in red.



(a)



(b)



(c)

Figure S3.2. ^1H -NMR spectrum of digested (a) EHU-30-NHR(Zr) and (b) EHU-30-NHR(Hf). (c) Label assignment of organic compounds: 2-aminobenzene-1,4-dicarboxylic acid in blue, 2-((2-carboxypropyl)amino)benzene-1,4-dicarboxylic acid in pink and methacrylic acid in orange.

S4. THERMOGRAVIMETRIC ANALYSIS OF EHU-30-NH₂ AND EHU-30-NHR

S4. THERMOGRAVIMETRIC ANALYSIS OF EHU-30-NH₂ AND EHU-30-NHR

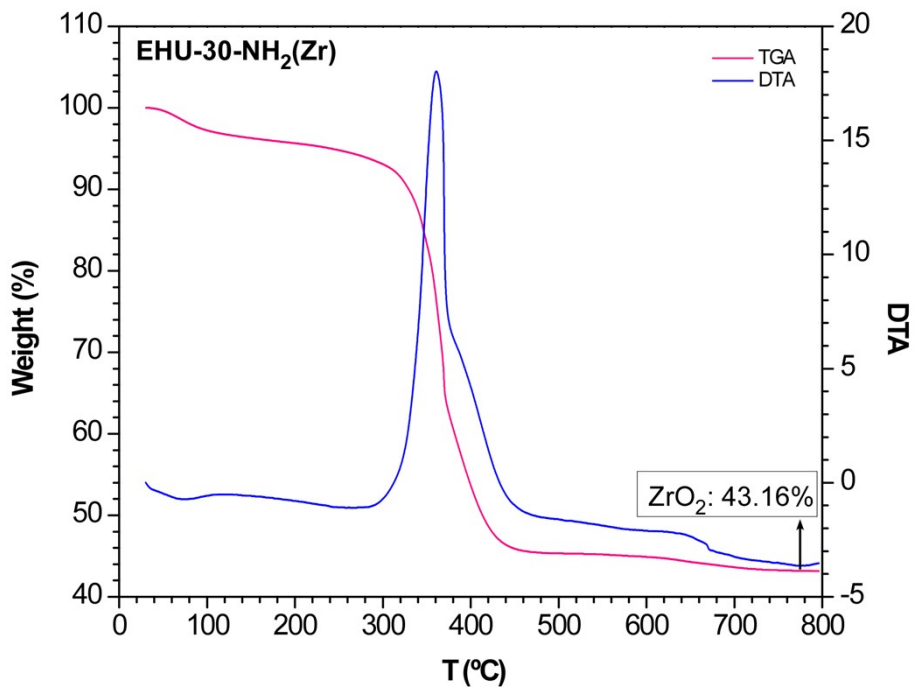
Thermogravimetric analysis of EHU-30-NH₂(M) and EHU-30-NHR(M) (M: Zr, Hf) were performed in synthetic air from 30 °C to 800 °C (Figures S4.1 and S4.2, respectively). In all compounds, the thermograms show two main weight loss stages. First, solvent and water molecules are released (25 – 130 °C). Thereafter, at 300 – 440 °C range, the framework decomposition takes place which it overlaps with the removal of monocarboxylate ligands (replacing the linkers). Note that with regard to the parent EHU-30, the amino group provides less thermal stability (see S5. Powder x-ray thermodiffraction of EHU-30-NH₂ and EHU-30-NHR), and do not allow to discriminate the removal of the monocarboxylate ligands.

In order to provide a more precise formula, we calculated the number of linker vacancies per Zr₆ formula unit based on thermogravimetric and ¹H-NMR analysis, considering two possibilities of defect compensating ligands (OH/H₂O and monocarboxylates that come from the modulator). The general defective formula for EHU-30-NH₂(M) is depicted by [M₆(OH)₄O₄(C₈H₅NO₄)_{6-x-y}(C₄H₇O₂)_{2x}(H₂O)_{2y}(OH)_{2y}]_n and for EHU-30-NHR(M), by [M₆(OH)₄O₄(C₈H₅NO₄)_{6-x-y-z}(C₁₂H₁₀NO₆)_z(C₄H₅O₂)_{2x}(H₂O)_{2y}(OH)_{2y}]_n. Both, the relative amount of the modulator and the amount of substituted linkers in EHU-30-NHR compounds, are subtracted from the integration of ¹H-NMR (see section S3), while the remaining values are fixed according to charge balance and thermogravimetric data. Further details are provided elsewhere.^{3,4} Accordingly, the following formulas were obtained:

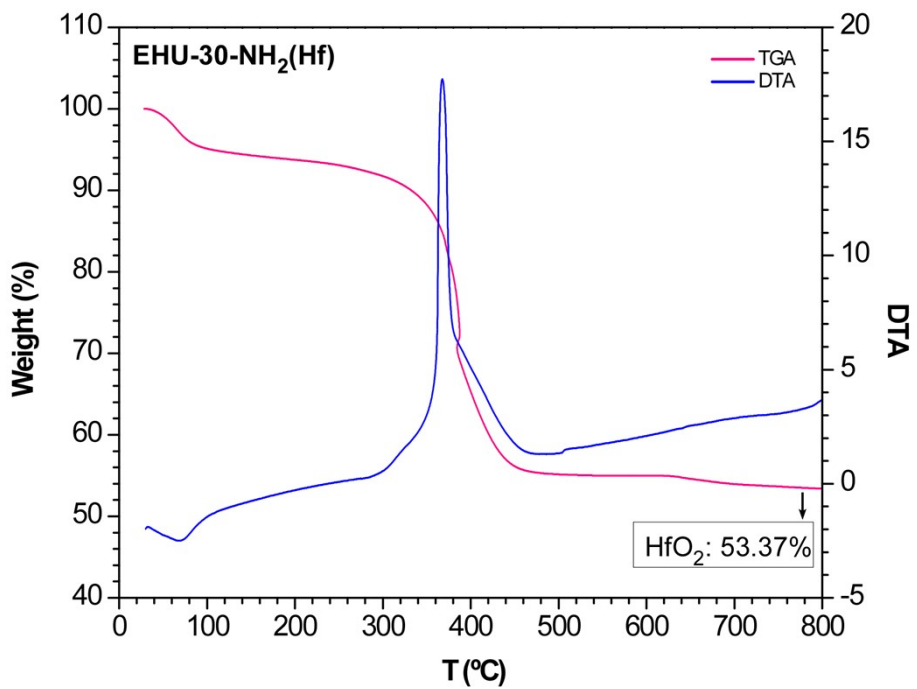
- **EHU-30-NH₂(Zr):** [Zr₆(OH)₄O₄(C₈H₅NO₄)_{4.76}(C₄H₇O₂)_{0.49}(H₂O)_{1.99}(OH)_{1.99}]_n (MW: 1644.59 g/mol)
- **EHU-30-NH₂(Hf):** [Hf₆(OH)₄O₄(C₈H₅NO₄)_{5.17}(C₄H₇O₂)_{0.71}(H₂O)_{0.95}(OH)_{0.95}]_n (MW: 2224.18 g/mol)
- **EHU-30-NHR(Zr):** [Zr₆(OH)₄O₄(C₈H₅NO₄)_{3.63}(C₁₂H₁₀NO₆)_{1.96}(C₄H₅O₂)_{0.47}(H₂O)_{0.35}(OH)_{0.35}]_n (MW: 1899.71 g/mol)
- **EHU-30-NHR(Hf):** [Hf₆(OH)₄O₄(C₈H₅NO₄)_{3.19}(C₁₂H₁₀NO₆)_{2.34}(C₄H₅O₂)_{0.69}(H₂O)_{0.25}(OH)_{0.25}]_n (MW: 2460.11 g/mol)

In both EHU-30-NH₂ compounds (Zr and Hf- based) a small fraction of 2-aminobenzene-1,4-dicarboxylate ligands has been replaced by isobutyrate ligands and OH/H₂O pairs, being the 21% for EHU-30-NH₂(Zr) and the 14% for EHU-30-NH₂(Hf). In EHU-30-NHR compounds same thing happens but being methacrylate the replacing ligand instead of isobutyrate, because it was the modulator employed in their synthesis and the responsible of the subreaction product leading to 2-((2-carboxypropyl)amino)benzene-1,4-dicarboxylate ligand. In this case, their formulas also show a good agreement to the ¹H-NMR ratios. In EHU-30-NHR(Zr) the 35% of dicarboxylate ligands has experienced the Aza-Michael reaction leading to the 2-carboxypropyl-amino derivative and the 7% of linker vacancies has been replaced by water/hydroxide pairs and methacrylate. In EHU-30-NHR(Hf) these values are 42% and 8%, respectively.

⁴ M. Taddei, G. M. Schukraft, M. E. A. Warwick, D. Tiana, M. J. McPherson, D. R. Jones and C. Petit, Band gap modulation in zirconium-based metal-organic frameworks by defect engineering, *J. Mater. Chem. A*, 2019, **7**, 23781-23786. <https://doi.org/10.1039/C9TA05216J>.

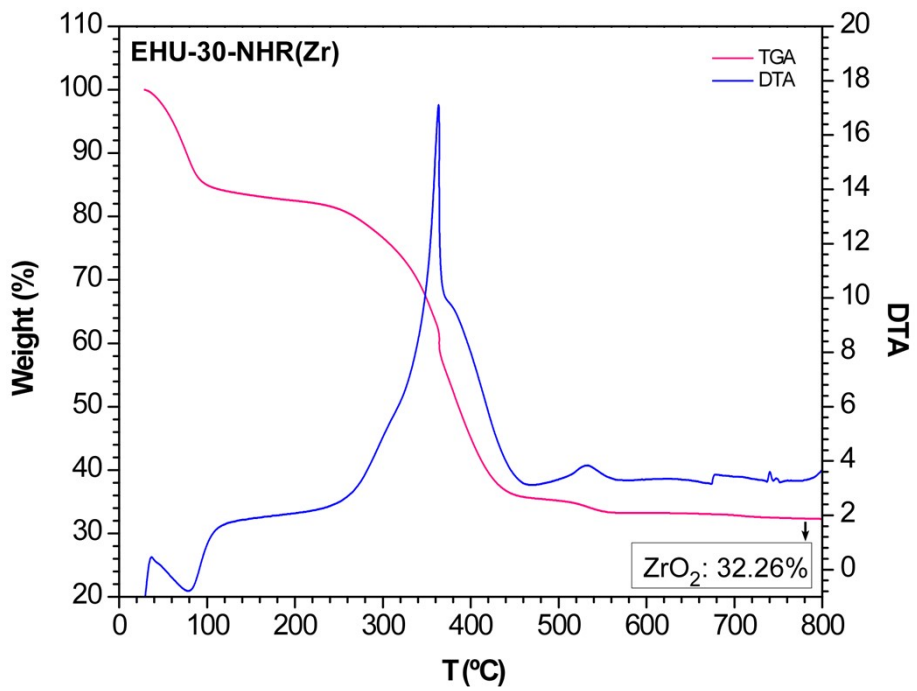


(a)

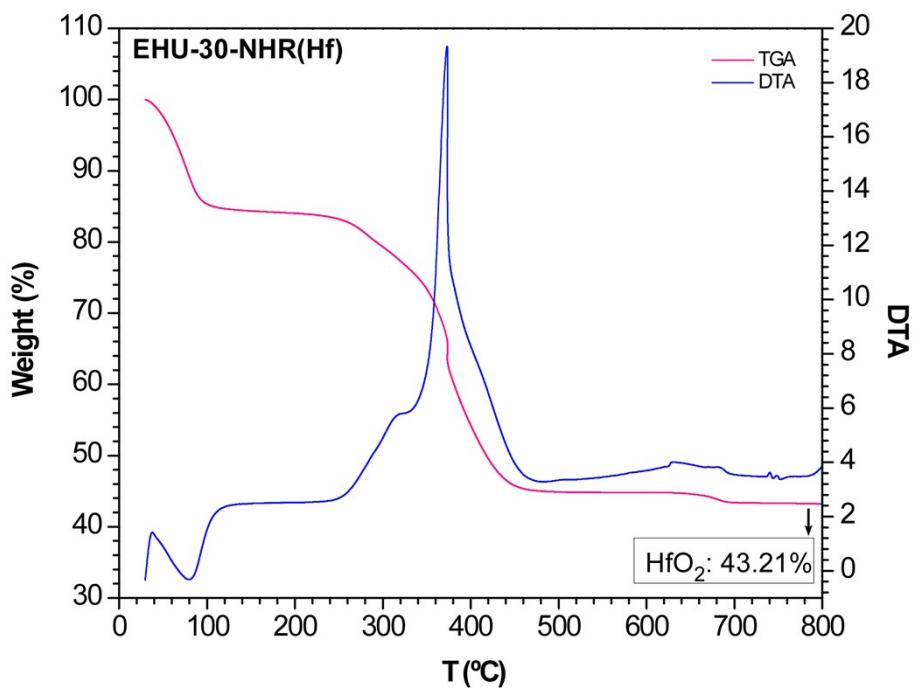


(b)

Figure S4.1. TGA-DTA curves of (a) EHU-30-NH₂(Zr) and (b) EHU-30-NH₂(Hf).



(a)



(b)

Figure S4.2. TGA-DTA curves of (a) EHU-30-NHR(Zr) and (b) EHU-30-NHR(Hf).

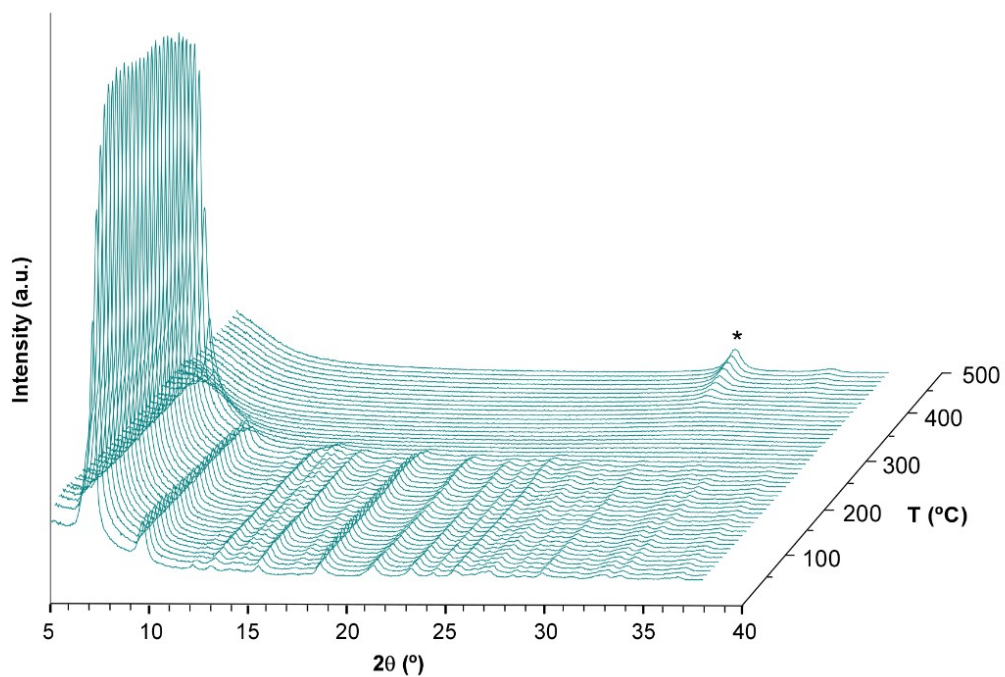
S5. POWDER X-RAY THERMODIFFRACTION (TDX) OF EHU-30-NH₂ AND EHU-30-NHR

S5. POWDER X-RAY THERMODIFFRACTION OF EHU-30-NH₂ AND EHU-30-NHR

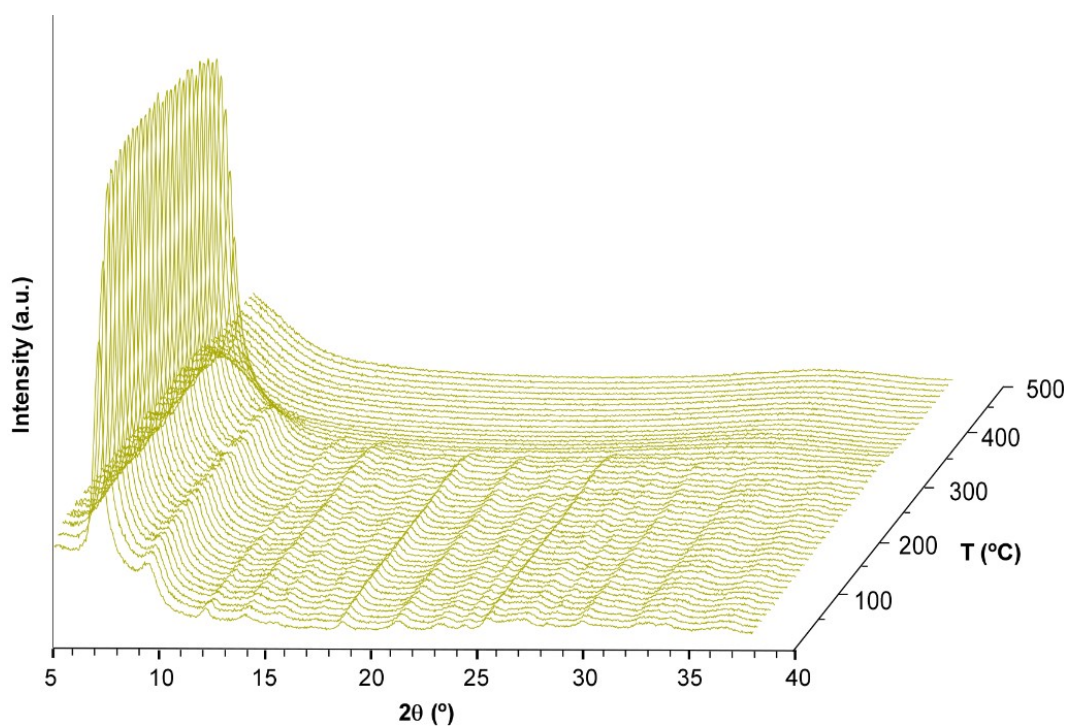
According to temperature variable PXRD experiments upon heating EHU-30-NH₂(M-based) and EHU-30-NHR(M-based, M = Zr or Hf) in Figures S5.1 and S5.2, respectively, any polymorphic phase transition towards a thermodynamically favoured phase was not observed. Probably because the strength of the zirconium/hafnium–oxygen bond imposes a too high activation energy barrier on this transition. All them exhibit a similar thermal stability being stable for up to *ca.* 300 °C after which it decomposes to yield ZrO₂/HfO₂. Above 400 °C, the emergence of a reflection corresponding to ZrO₂ can be observed. This is in concordance with TGA analysis, and compared to EHU-30(Zr) (with a thermal stability up to 450 °C)⁵ the difference relies on the amino-functionalization of the organic linker, which offers less stability to the resulting compounds, as it has also been observed in UiO-66-NH₂ with a thermal stability of *ca.* 300°C.⁶

⁵ M. Perfecto-Irigaray, G. Beobide, O. Castillo, I. Da Silva, D. García-Lojo, A. Luque, A. Mendia and S. Pérez-Yáñez, [Zr₆O₄(OH)₄(Benzene-1,4-Dicarboxylato)₆]_n: A Hexagonal Polymorph of UiO-66, *Chem. Commun.*, 2019, **55**, 5954–5957. <https://doi.org/10.1039/c9cc00802k>.

⁶ M. Kandiah, M. H. Nilsen, S. Usseglio, S. Jakobsen, U. Olsbye, M. Tilset, Ch. Larabi, E. A. Quadrelli, F. Bonino and K. P. Lillerud, Synthesis and Stability of Tagged UiO-66 Zr-MOFs, *Chem. Mater.*, 2010, **22**, 6632–6640. <https://doi.org/10.1021/cm102601v>

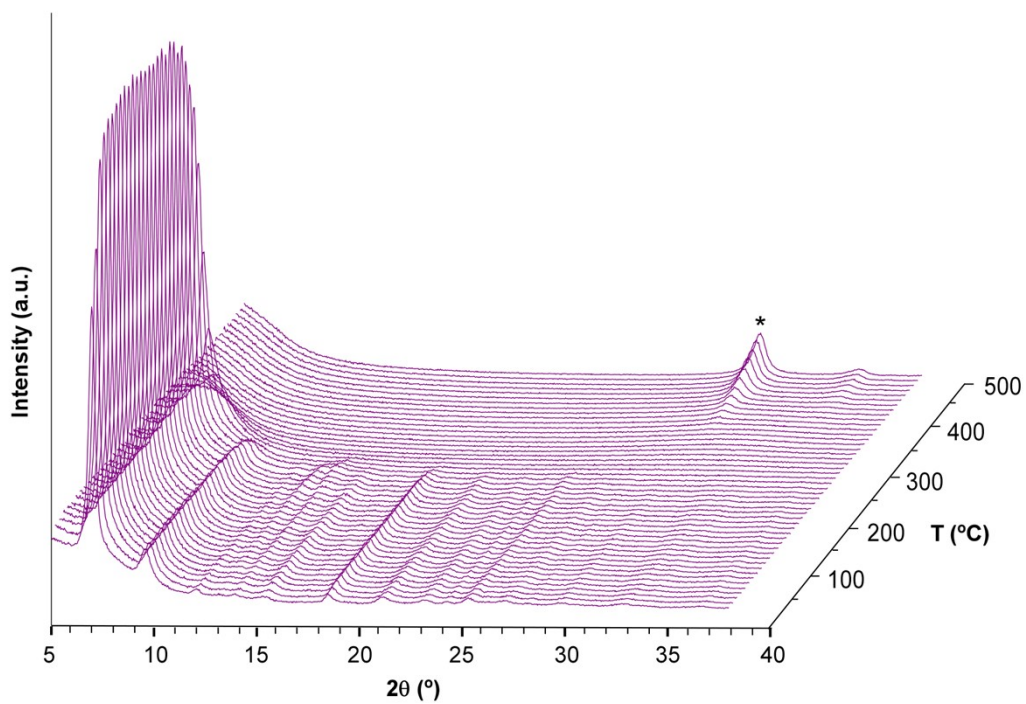


(a)

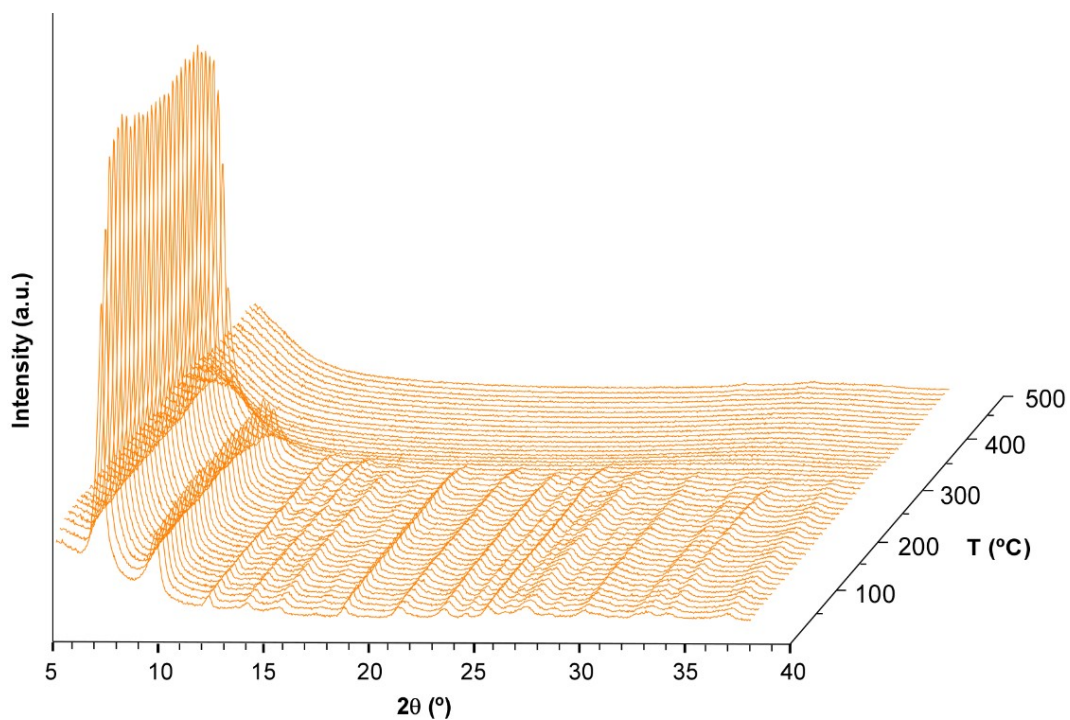


(b)

Figure S5.1. Variable-temperature PXRD patterns of (a) EHU-30-NH₂(Zr) and (b) EHU-30-NH₂(Hf) measured from 30 to 500 °C each 10 °C at air atmosphere.



(a)

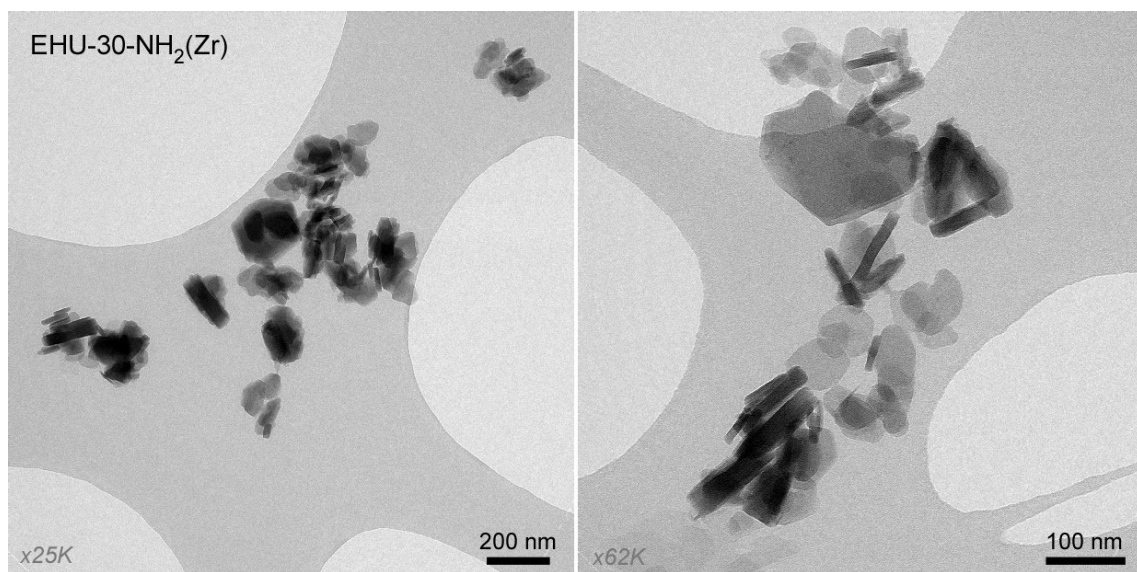


(b)

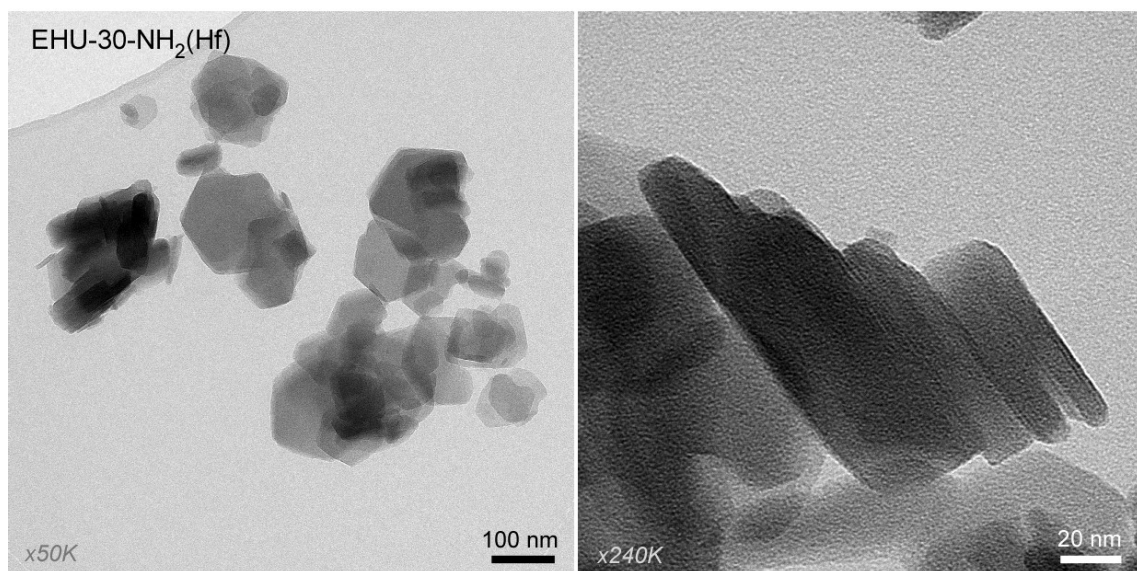
Figure S5.2. Variable-temperature PXRD patterns of (a) EHU-30-NHR(Zr) and (b) EHU-30-NHR(Hf) measured from 30 to 500 $^\circ\text{C}$ each 10 $^\circ\text{C}$ at air atmosphere.

S6. TEM AND SEM MICROGRAPHS OF EHU-30-NH₂ AND EHU-30-NHR

S6. TEM AND SEM MICROGRAPHS OF EHU-30-NH₂ AND EHU-30-NHR

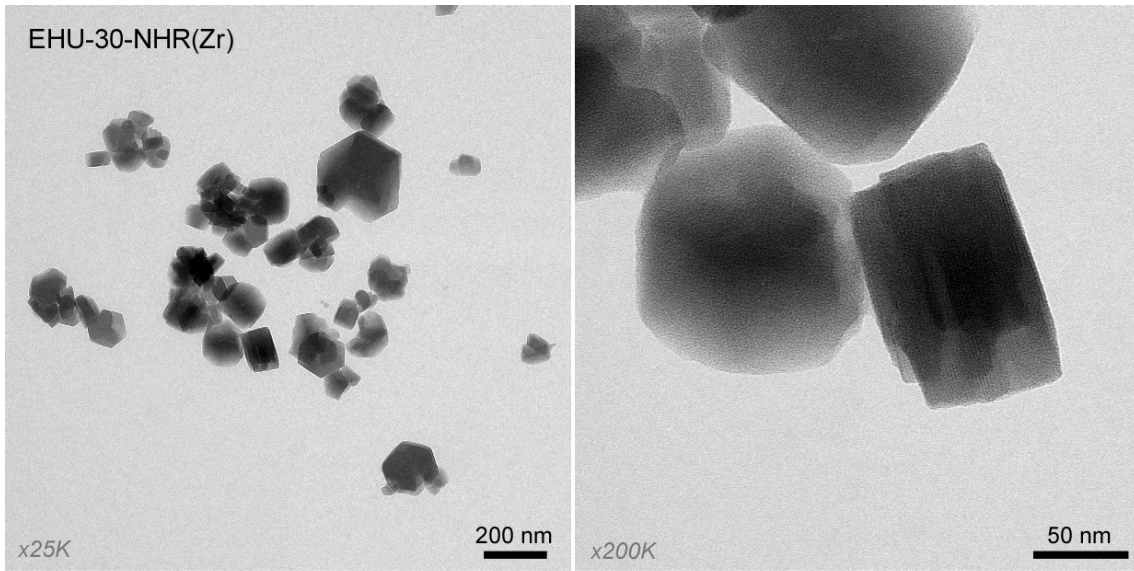


(a)

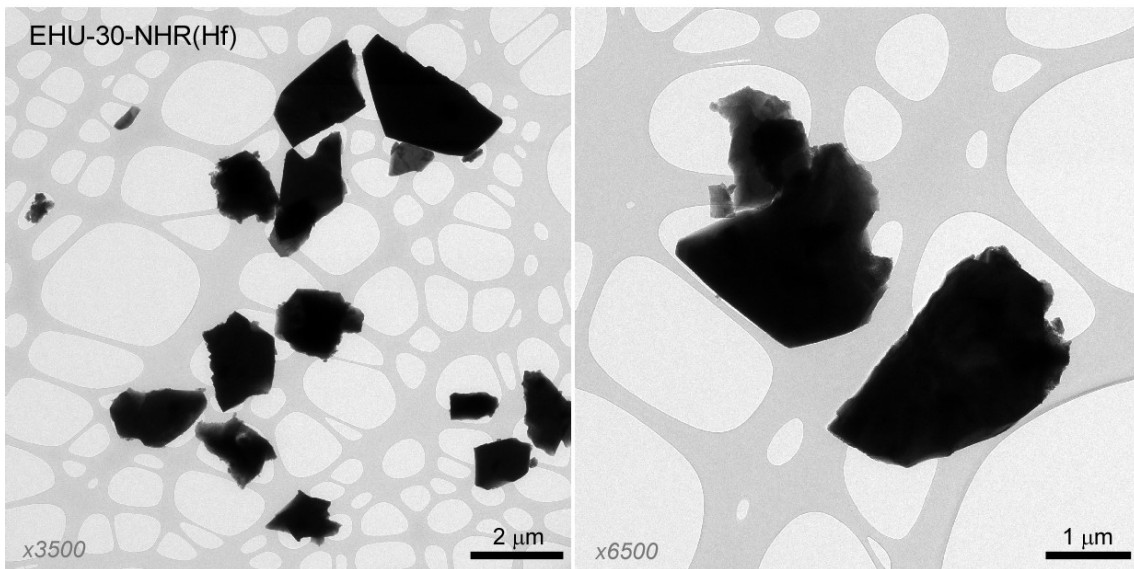


(b)

Figure S6.1. Transmission electron microscopy images taken on (a) EHU-30-NH₂(Zr) and (b) EHU-30-NH₂(Hf).



(a)



(b)

Figure S6.2. Transmission electron microscopy images taken on (a) EHU-30-NHR(Zr) and (b) EHU-30-NHR(Hf).

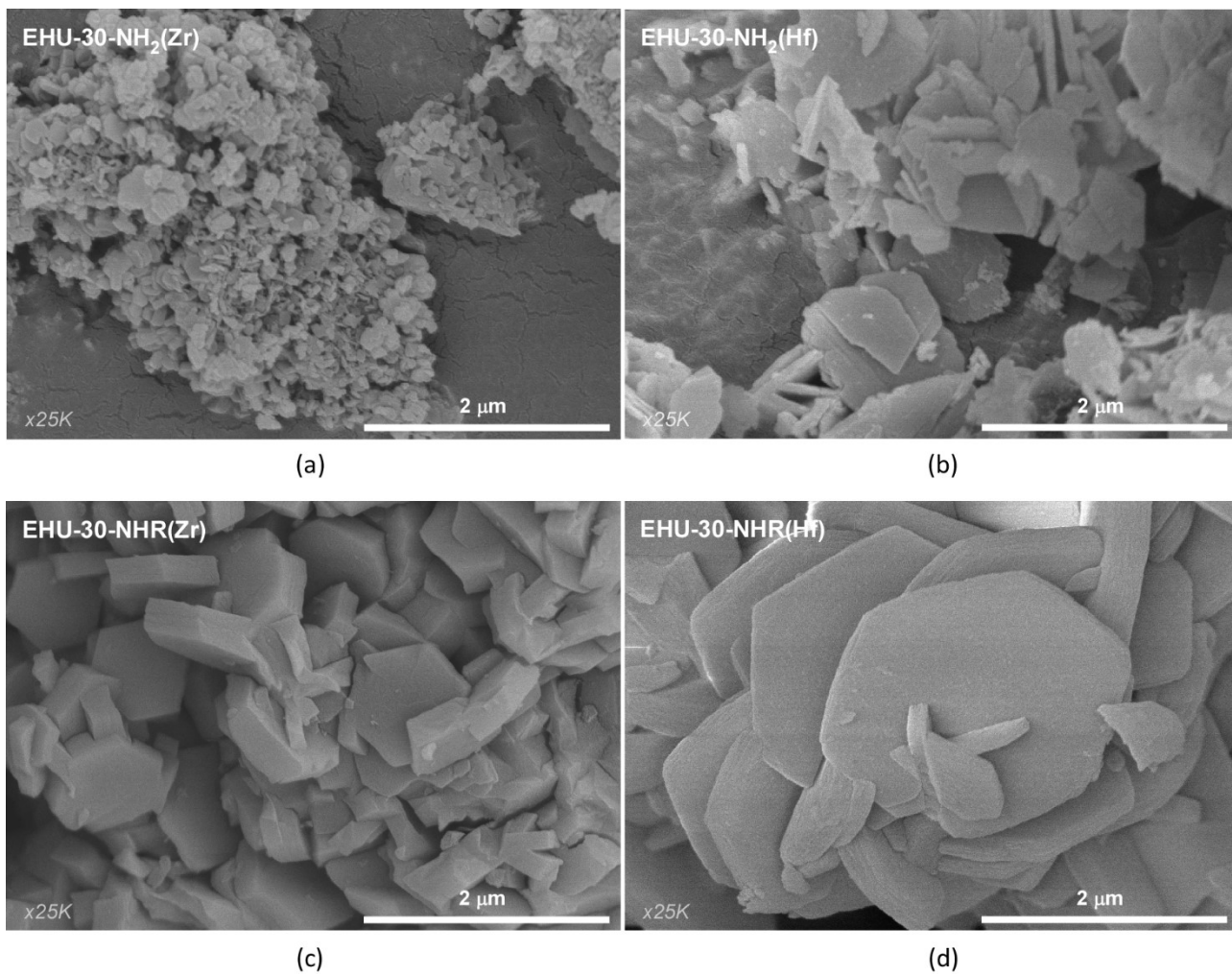


Figure S6.3. Scanning electron microscopy images taken at 25K magnification on (a) EHU-30-NH₂(Zr), (b) EHU-30-NH₂(Hf), (c) EHU-30-NHR(Zr) and (d) EHU-30-NHR(Hf).

S7. CRYSTAL STRUCTURE ELUCIDATION

S7. CRYSTAL STRUCTURE ELUCIDATION

Powder X-ray diffraction patterns of polycrystalline EHU-30-NH₂(Zr) and EHU-30-NH₂(Hf) were measured on a Bruker D8 Advance diffractometer, equipped with a 1-D LynxEye detector, and using Cu K α ₁ radiation. Samples were mounted on zero-background silicon sample holders and data was collected at 293 K.

Crystal structures of both EHU-30-NH₂(Zr) and EHU-30-NH₂(Hf) were refined using Topas Academic v6 program. The crystal structure of EHU-30(Zr) was taken as starting point, where an amino group was introduced, replacing one of the BDC hydrogen atoms.

Final Rietveld refinements of EHU-30-NH₂(Zr) and EHU-30-NH₂(Hf) crystal structures were carried out in the 2 θ ranges 5-70° and 5-78° (up to about 1.34 and 1.22 Å in *d*-spacing), respectively, and atomic coordinates of all atoms were included. For each refinement, an isotropic atomic displacement parameter was applied for the metal atom, while an overall parameter was introduced for the light atoms (excluding the N atom). On the final fits, there were 90 and 83 different adjustable parameters, respectively (scale factor, zero shift, background, unit-cell parameters, peak-shape parameters, atomic coordinates, and temperature factors). Figures S7.1 and S7.2 show the final Rietveld fits for EHU-30-NH₂(Zr) and EHU-30-NH₂(Hf), respectively. Table S7.1 summarizes the corresponding crystallographic and refinement-related data, while final atomic coordinates obtained for non-H atoms are reported in Tables S7.2 and S7.3.

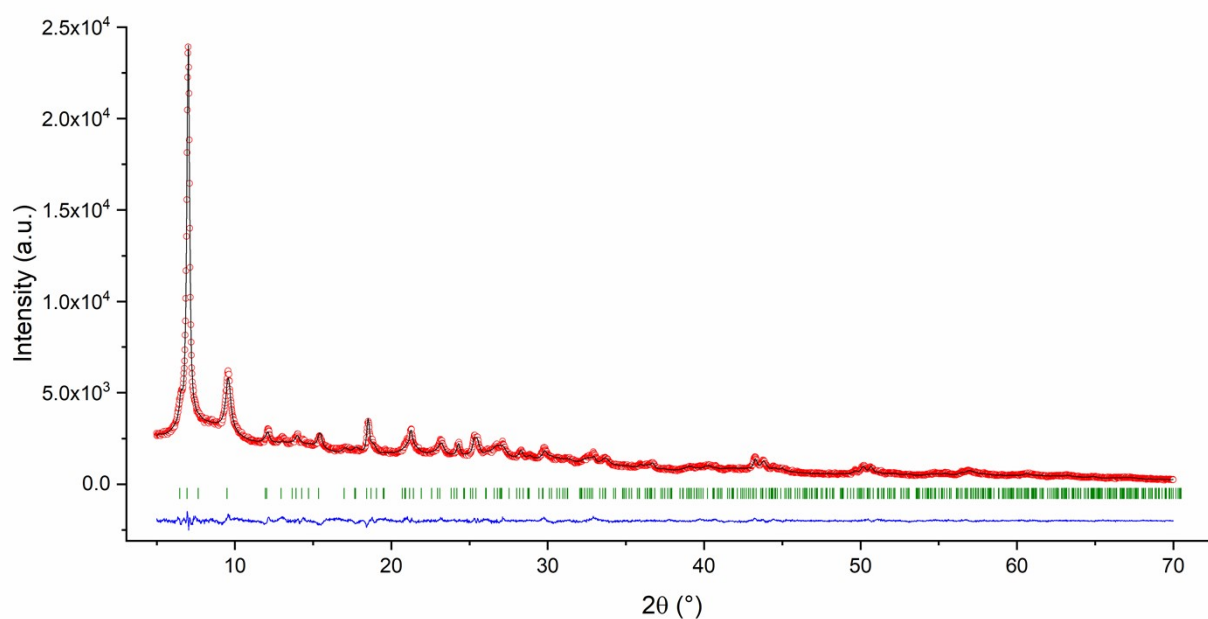


Figure S7.1. Final Rietveld refinement plot for EHU-30-NH₂(Zr), showing the experimental (red circles), calculated (black line), and difference profiles (blue line); green tick marks indicate reflection positions.

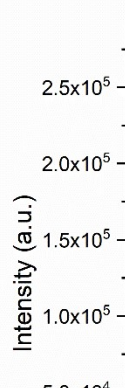


Figure S7.2. Final Rietveld refinement plot for EHU-30-NH₂(Hf), showing the experimental (red circles), calculated (black line), and difference profiles (blue line); green tick marks indicate reflection positions.

Table S7.1. Crystallographic data and Rietveld refinement summary for EHU-30-NH₂(Zr) and EHU-30-NH₂(Hf).

Compound	EHU-30-NH ₂ (Zr)	EHU-30-NH ₂ (Hf)
Formula	[Zr ₆ (C ₈ H ₅ NO ₄) ₆ (O) ₄ (OH) ₄]	[Hf ₆ (C ₈ H ₅ NO ₄) ₆ (O) ₄ (OH) ₄]
Formula weight (g/mol)	1750.1	2273.72
<i>D_c</i> (g/cm ³)	1.136	1.516
Crystal system	Hexagonal	Hexagonal
Space group	<i>P6₃/mmc</i>	<i>P6₃/mmc</i>
<i>a</i> (Å)	14.7044(12)	14.6647(5)
<i>c</i> (Å)	27.320(7)	26.744(7)
<i>V</i> (Å ³)	5115.7(15)	4980.8(14)
<i>Z</i>	2	2
Radiation type	X-ray tube, Cu Kα ₁	X-ray tube, Cu Kα ₁
Diffractometer	Bruker D8 Advance	Bruker D8 Advance
Data collection mode	Reflection	Reflection
Wavelength (Å)	1.540596	1.540596
<i>R_p</i> (%)	2.99	4.52
<i>R_{wp}</i> (%)	3.92	5.94
<i>R_{exp}</i> (%)	2.60	1.21
<i>R_B</i> (%)	0.97	1.76
<i>Goodness-of-fit</i>	1.51	4.90

Table S7.2. Fractional atomic coordinates and isotropic displacement parameter (\AA^2) of non-H atoms for EHU-30-NH₂(Zr).

Atom	x	y	z	B _{iso}	Occupancy
Zr1	0.8336(6)	-0.0832(3)	0.0505(5)	0.5(2)	1
O1	0.820(4)	-0.0901(18)	-0.032(4)	6.4(8)	1
O2	1	0	0.066(6)	6.4(8)	1
C1_1	0.515(3)	-0.063(5)	0.034(2)	6.4(8)	1
C3_1	0.5948(13)	0	0	6.4(8)	1
C4_1	0.696(3)	0	0	6.4(8)	1
O5_1	0.707(7)	-0.060(8)	0.033(2)	6.4(8)	1
N1_1	0.530(5)	-0.127(8)	0.070(3)	7.7(9)	0.25
C1_2	0.815(4)	-0.205(3)	0.2243(13)	6.4(8)	1
C3_2	0.898(3)	-0.205(6)	0.19857261(9)	6.4(8)	1
C4_2	0.907(6)	-0.186(12)	0.1461(3)	6.4(8)	1
O5_2	0.851(9)	-0.159(9)	0.123(4)	6.4(8)	1
N1_2	0.739(5)	-0.187(6)	0.1984(19)	7.7(9)	0.25

Table S7.3. Fractional atomic coordinates and isotropic displacement parameter (\AA^2) of non-H atoms for EHU-30-NH₂(Hf).

Atom	x	y	z	B _{iso}	Occupancy
Hf1	0.8380(5)	-0.0810(2)	0.0551(5)	1.89(19)	1
O1	0.858(6)	-0.071(3)	-0.023(6)	8.1(11)	1
O2	1	0	0.071(9)	8.1(11)	1
C1_1	0.523(3)	-0.050(4)	0.039(2)	8.1(11)	1
C3_1	0.5958(14)	0	0	8.1(11)	1
C4_1	0.698(3)	0	0	8.1(11)	1
O5_1	0.717(8)	-0.046(9)	0.035(3)	8.1(11)	1
N1_1	0.546(5)	-0.102(8)	0.079(3)	9.7(13)	0.25
C1_2	0.816(4)	-0.201(3)	0.2237(16)	8.1(11)	1
C3_2	0.899(4)	-0.201(8)	0.197464259(6)	8.1(11)	1
C4_2	0.909(8)	-0.182(16)	0.1439(4)	8.1(11)	1
O5_2	0.853(11)	-0.156(11)	0.120(5)	8.1(11)	1
N1_2	0.740(6)	-0.184(6)	0.197(2)	9.7(13)	0.25

S8. COMPUTATIONAL DETAILS

S8. COMPUTATIONAL DETAILS

Simulation of adsorption isotherms

Adsorption isotherms of pure components (CO₂ and N₂) and binary mixtures (water and N₂) were calculated using the software package RASPA.⁷ We used Grand Canonical Monte Carlo simulations, where chemical potential, volume, and temperature were kept fixed. We used the Peng-Robinson equation and the fugacity coefficient to relate the chemical potential to pressure. Absolute loading (n_{abs}) obtained in the simulations was converted to excess loading (n_{exc}) by using the following equation:

$$n_{exc} = n_{abs} - V^g \rho^g$$

where V^g is the pore volume of the adsorbent and ρ^g is the molar density of the bulk gas phase.⁸

During the simulation, system configurations are generated by randomly selecting a molecule and applying random moves. These moves can be rotation, translation, regrow, insertion/deletion, and identity change in the case of mixtures. At least 4×10^5 equilibration steps and 6×10^6 production steps were used to ensure equilibrium in case of single gas isotherm. For the binary mixtures at least 10^6 and 10^7 steps for equilibration and production were used. We used Lennard-Jones (L-J) and Coulombic potentials to define the interactions between the atoms of the system and generic Lorentz-Berthelot mixing rules were applied to compute guest-guest and host-guest L-J interactions. The Ewald summation method is employed to calculate the Coulombic interactions with a relative precision of 10^{-6} . L-J and Coulombic potentials were cut and shifted at a cut off distance of 12 Å. We used periodic boundary conditions and the simulation box contained as many unit cells of each structure as needed to ensure that the dimensions of the simulation box are at least twice the cut off.

For CO₂, we used the model developed by García-Sánchez et al.⁹ which is a rigid full atom model with C-O distance = 1.149 Å. For N₂ we used the model reported by Martín-Calvo et al.¹⁰ consisting of two Lennard-Jones interaction centres at a distance of 1.10 Å and an additional dummy bead placed at the centre of mass of the molecule. In the case of water, we used the Tip4pEw model. It is a rigid planar four-site interaction model consisting of a single Lennard-Jones interaction centre located at the atom of oxygen while the atoms of hydrogen and the dummy bead have charges.¹¹ All Lennard-Jones parameters and charges of the models used for the gases are listed in Table S8.1.

⁷ D. Dubbeldam, S. Calero, D. E. Ellis and R. Q. Snurr, . RASPA: Molecular Simulation Software for Adsorption and Diffusion in Flexible Nanoporous Materials, *Mol. Simul.*, 2016, **42**, 81–101. <https://doi.org/10.1080/08927022.2015.1010082>

⁸ O. Talu and A. L. Myers, Molecular Simulation of Adsorption: Gibbs Dividing Surface and Comparison with Experiment, *AIChE J.*, 2001, **47**, 1160–1168. <https://doi.org/10.1002/aic.690470521>.

⁹ A. García-Sánchez, C. O. Ania, J. B. Parra, D. Dubbeldam, T. J. H. Vlugt, R. Krishna and S. Calero, . Transferable Force Field for Carbon Dioxide Adsorption in Zeolites, *J. Phys. Chem. C.*, 2009, **113**, 8814–8820. <https://doi.org/10.1021/jp810871f>.

¹⁰ A. Martín-Calvo, E. García-Pérez, A. García-Sánchez, R. Bueno-Pérez, S. Hamad and S. Calero, Effect of Air Humidity on the Removal of Carbon Tetrachloride from Air Using Cu-BTC Metal-Organic Framework, *Phys. Chem. Chem. Phys.*, 2011, **13**, 11165–11174. <https://doi.org/10.1039/c1cp20168a>.

¹¹ H. W. Horn, W. C. Swope, J. W. Pitera, J. D. Madura, T. J. Dick, G. L. Hura and T. Head-Gordon, . Development of an Improved Four-Site Water Model for Biomolecular Simulations: TIP4P-Ew, *J. Chem. Phys.*, 2004, **120**, 9665–9678. <https://doi.org/10.1063/1.1683075>.

To model the structures, we used the crystallographic position of the atoms obtained from the crystal structure of the materials. The hydrogen atoms of the hydroxide groups were geometrically sited with a $d_{\text{O-H}} = 0.94 \text{ \AA}$ and $\text{M-O-H} = 111\text{-}112^\circ$. The structures are considered as rigid frameworks with Lennard-Jones and point charges assigned. Most L-J parameters are taken from DREIDING force field¹² except those for the metal atoms that are taken from UFF force field.¹³ The point charges to model the electrostatic potential of the adsorbents were previously calculated by means of Density Functional Theory (DFT) calculations using the ESP method as described by Singh and Kollman,¹⁴ which is implemented in the DMOL3 code.¹⁵ To accomplish the DFT calculations DNP basis set and the PBE exchange-correlation functional were employed.¹⁶ To conduct the ESP charge calculations neutral finite cluster models of formula $[\text{M}_6\text{O}_4(\text{OH})_4(\text{L})_{12}]$ (M: Zr, Hf; L: BDC, $\text{NH}_2\text{-BDC}$) were built for each MOF (Figures S8.1 and 8.3) All Lennard-Jones parameters are listed in Table S8.1 while the charges of the atoms are included in the Tables S8.2 to S8.5.

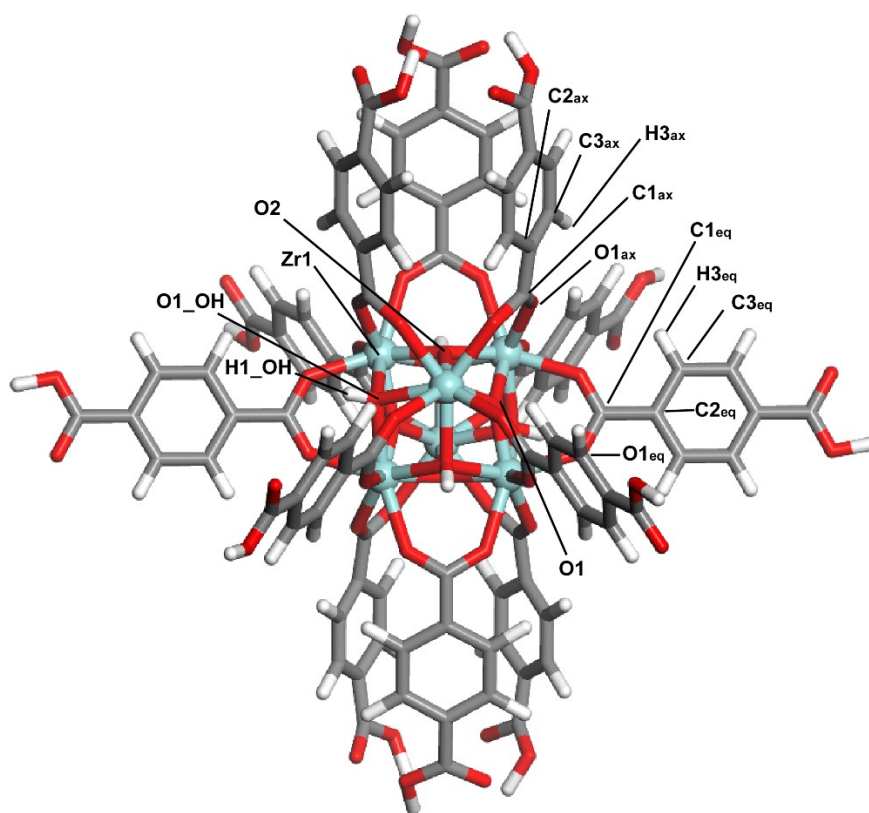


Figure S8.1. Finite cluster model of EHU-30(Zr) employed to calculate the ESP charges and labelling of the atoms.

¹² S. L. Mayo, B. D. Olafson and W. A. Goddard, DREIDING: A Generic Force Field for Molecular Simulations, *J. Phys. Chem.*, 1990, **94**, 8897–8909. <https://doi.org/10.1021/j100389a010>

¹³ A. K. Rappé, C. J. Casewit, K. S. Colwell, W. A. Goddard III and W. M. Skiff, UFF, a Full Periodic Table Force Field for Molecular Mechanics and Molecular Dynamics Simulations, *J. Am. Chem. Soc.*, 1992, **114**, 100021–110035. https://doi.org/10.1007/978-3-642-04431-1_17

¹⁴ U. C. Singh and P. A. Kollman, An approach to computing electrostatic charges for molecules, *J. Comput. Chem.*, 1984, **5**, 129–145. <https://doi.org/10.1002/jcc.540050204>

¹⁵ B. Delley, From molecules to solids with the DMOL3 approach, *J. Chem. Phys.*, 2000, **113**, 7756–7765. <https://doi.org/10.1063/1.1316015>

¹⁶ J. P. Perdew, K. Burke and M. Ernzerhof, Generalized Gradient Approximation Made Simple, *Phys. Rev. Lett.*, 1996, **77**, 3865–3868. <https://doi.org/10.1103/PhysRevLett.77.3865>

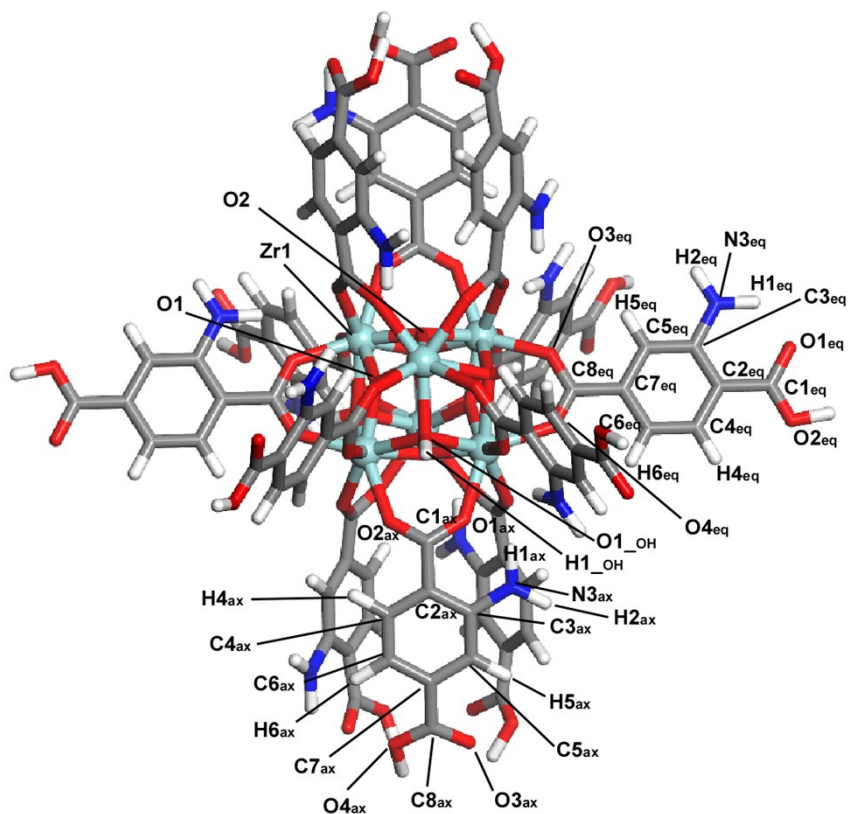


Figure S8.2. Finite cluster model of EHU-30-NH₂(Zr) employed to calculate the ESP charges and labelling of the atoms. Same finite cluster and labels were established for EHU-30-NH₂(Hf), but changing Zr1 by Hf1.

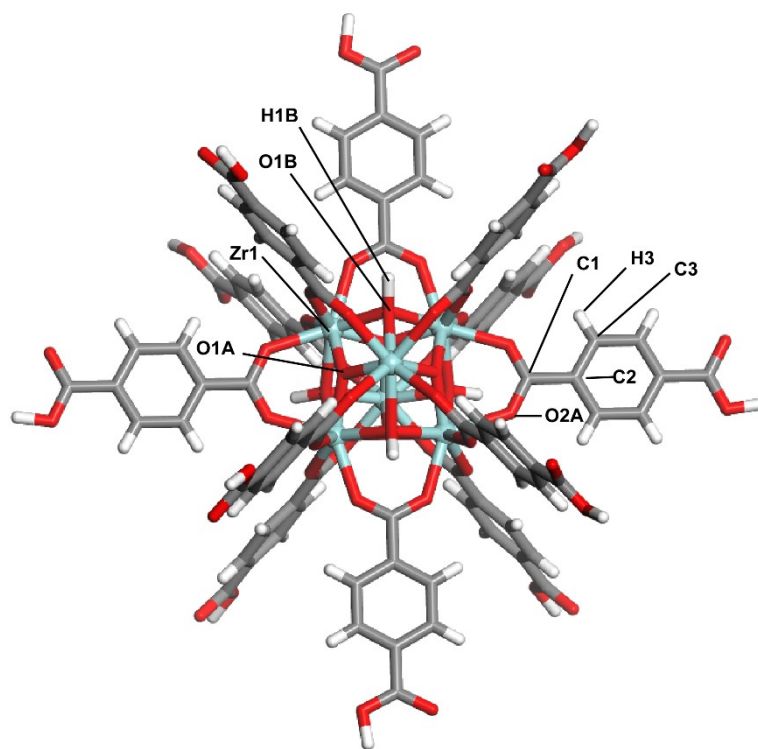


Figure S8.3. Finite cluster model of UiO-66(Zr) employed to conduct the ESP charges and labelling of the atoms.

Table S8.1. Lennard Jones parameters employed in the simulations.

Interaction centre	ϵ/k_B [K]	σ [Å]	q [e]
C_CO2	29.933	2.742	0.6512
O_CO2	85.671	3.017	-0.3256
N_N2	38.298	3.306	-0.40484
Dummy_N2	-	-	0.8096
O_water	81.899	3.164	0
H_water	-	-	0.524
Dummy_water	-	-	-1.048
Hf_framework	36.269	2.798	Tables S8.2 to S8.4
Zr_framework	34.722	2.783	
C_framework	47.86	4.473	
O_framework	48.19	3.033	
H_framework	7.65	2.846	
N_framework	38.949	3.262	

Table S8.2. ESP charges (q / e) for the atoms of the structural model of EHU-30(Zr).

EHU-30			
Cluster		Equatorial BDC	
atom	charge	atom	charge
Zr1	2.4325087070470	C1eq	0.9545087218285
O1	-1.0834912061690	C2eq	-0.1124912351370
O2	-0.8094912767410	C3eq	-0.1214912310243
O1_OH	-1.1994911432270	H3eq	0.1605087667704
H1_OH	0.5355087518692	O1eq	-0.8224912285805
Axial BDC (triad)			
atom	charge	atom	charge
C1ax	0.6455087661743	H3ax	0.1145087629557
C2ax	-0.1484912335873	O1ax	-0.6194912195206
C3ax	-0.0604912340641		

Table S8.3. ESP charges (q / e) for the atoms of the structural model of tEHU-30-NH₂(Zr).

EHU-30-NH ₂ (Zr)	
Cluster	

atom	charge	atom	charge
Zr1	2.3109524250030	O1_OH	-1.0730476379390
O1	-1.1180477142330	H1_OH	0.4759523570538
O2	-0.9130476117134		
Equatorial NH₂-BDC			
atom	charge	atom	charge
O1eq	-0.8030475974083	H4eq	0.1709523797035
O2eq	-0.8590475916862	C5eq	-0.3550476431847
C1eq	1.1119523048400	H5eq	0.2199523746967
C2eq	-0.4420476257801	C6eq	-0.2060476243496
C3eq	0.6229524016380	H6eq	0.1719523817301
N3eq	-1.0610476732250	C7eq	-0.1320476233959
H1eq	0.4699523746967	C8eq	1.0859522819520
H2eq	0.4289523661137	O3eq	-0.8940476179123
C4eq	-0.0530476197600	O4eq	-0.8200476169586
Axial NH₂-BDC (triad)			
atom	charge	atom	charge
O1ax	-0.3630476295948	H4ax	0.1379523873329
O2ax	-0.5110476016998	C5ax	-0.3840476274490
C1ax	0.4629523754120	H5ax	0.1639523804188
C2ax	-0.2280476242304	C6ax	-0.2550476193428
C3ax	0.6339523792267	H6ax	0.1499523818493
N3ax	-1.1580476760860	C7ax	-0.0150476172566
H1ax	0.4299523532391	C8ax	0.6019523739815
H2ax	0.4589523673058	O3ax	-0.5700476169586
C4ax	-0.1100476160645	O4ax	-0.5740476250648

Table S8.4. ESP charges (q / e) for the atoms of the structural model of EHU-30-NH₂(Hf).

EHU-30-NH₂(Hf)			
Cluster			
atom	charge	atom	charge
Hf1	2.0369682312010	O1_OH	-0.9790318012238
O1	-0.9750317931175	H1_OH	0.4659682512283
O2	-0.7750317454338		
Equatorial NH₂-BDC			
atom	charge	atom	charge
O1eq	-0.7490317821503	H4eq	0.1699682623148

O2eq	-0.7940317988396	C5eq	-0.3560317456722
C1eq	1.0719683170320	H5eq	0.2179682552814
C2eq	-0.4480317533016	C6eq	-0.2500317394733
C3eq	0.6439682245255	H6eq	0.1749682575464
N3eq	-1.0880317687990	C7eq	-0.1180317550898
H1eq	0.4899682700634	C8eq	1.0379682779310
H2eq	0.4359682500362	O3eq	-0.8500317931175
C4eq	-0.0520317479968	O4eq	-0.7420317530632
Axial NH₂-BDC (triad)			
atom	charge	atom	charge
O1ax	-0.2960317432880	H4ax	0.1399682611227
O2ax	-0.4330317378044	C5ax	-0.4350317418575
C1ax	0.3649682700634	H5ax	0.1749682575464
C2ax	-0.1800317466259	C6ax	-0.2830317318439
C3ax	0.6299682259560	H6ax	0.1539682596922
N3ax	-1.1840317249300	C7ax	0.0609682537615
H1ax	0.4459682703018	C8ax	0.4979682564735
H2ax	0.4699682593346	O3ax	-0.4890317320824
C4ax	-0.1320317387581	O4ax	-0.5250317454338

Table S8.5. ESP charges (q / e) for the atoms of the structural model of UiO-66(Zr).

EHU-30			
Cluster		Equatorial BDC	
atom	charge	atom	charge
Zr1	2.5890879631040	C1	0.8610876798630
O1A	-1.0379120111470	C2	-0.1529123038054
O1B	-1.5949120521550	C3	-0.0864122733474
H1B	0.5800877213478	H3	0.1530877053738
		O2A	-0.7259122729301

S9. GAS ADSORPTION DATA

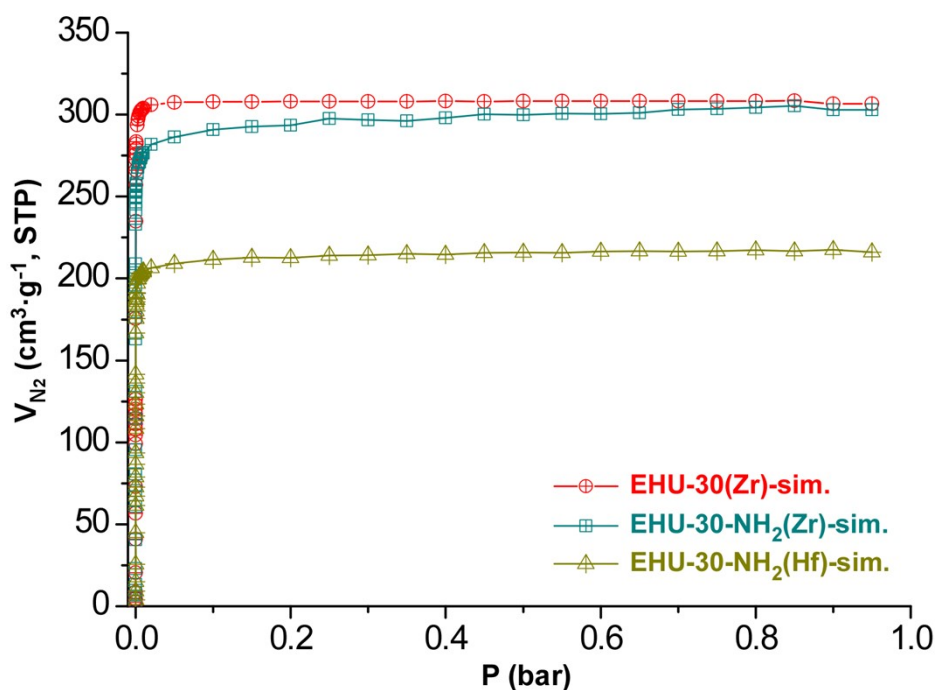
Simulated N₂ adsorption isotherms

Figure S9.1. Simulated N₂ isotherms at 77K of EHU-30(Zr), EHU-30-NH₂(Zr) and EHU-30-NH₂(Hf).

BET fitting of simulated and experimental isotherms

The surface area values were calculated by fitting the adsorption data to Brunauer-Emmett-Teller (BET) equation S7.1:¹⁷

$$\frac{P/P_0}{V(1 - P/P_0)} = \frac{1}{V_m C} + \frac{C - 1}{V_m C} (P/P_0) \quad \text{Equation S9.1}$$

where V is the specific amount adsorbed at the relative pressure P/P₀, V_m is the specific amount adsorbed corresponding to the monolayer formation and C is a parameter exponentially related to the energy of monolayer formation.

Regarding the application of the BET method to microporous materials,¹⁸ to avoid ambiguity when reporting the surface area of microporous MOFs, the pressure range for the data fitting was set according the consistency criteria proposed by Rouquerol et al.:¹⁹

- (1) The pressure range selected should have values of V(1 – P/P₀) increasing with P/P₀.

¹⁷ S. Brunauer, P. H. Emmett and E. J. Teller, Adsorption of Gases in Multimolecular Layers, *Am. Chem. Soc.*, 1938, **60**, 309–319. <https://doi.org/10.1021/ja01269a023>

¹⁸ M. Thommes, K. Kaneko, A. V. Neimark, J. P. Oliver, F. Rodriguez-Reinoso, J. Rouquerol and K. S. W. Sing, . Physisorption of Gases, with Special Reference to the Evaluation of Surface Area and Pore Size Distribution (IUPAC Technical Report), *Pure Appl. Chem.*, 2015, **87**, 1051–1069. <https://doi.org/10.1515/pac-2014-1117>

¹⁹ J. Rouquerol, P. Llewellyn and F. Rouquerol, Is the bet equation applicable to microporous adsorbents?, *Stud. Surf. Sci. Catal.*, 2007, **160**, 49–56. [https://doi.org/10.1016/S0167-2991\(07\)80008-5](https://doi.org/10.1016/S0167-2991(07)80008-5)

(2) The points used to calculate the BET surface area must be linear with an upward slope in such a way that the linear regression must yield a positive y-intercept (i.e. positive C value).

(3) The P/P_0 value corresponding to V_m should be within the BET fitting range.

Note that the BET surface area calculated from a Type I isotherm must not be considered as a real accessible surface area,²⁰ but it must be taken as an apparent surface area. In any case, the above described criteria allows to estimate an area that can be regarded as an useful adsorbent “fingerprint”, as it avoids a doubtful selection of the fitting range. In fact, this procedure is commonly applied to calculate the BET surface area values of MOFs.²¹

According to the aforementioned first consistency criteria, $V(1 - P/P_0)$ vs P/P_0 plots (Figure S9.2) were used to define the pressure range. Second and third criteria were as well fulfilled upon selected fitting range. Resulting BET fitting data are gathered in Table S9.1.

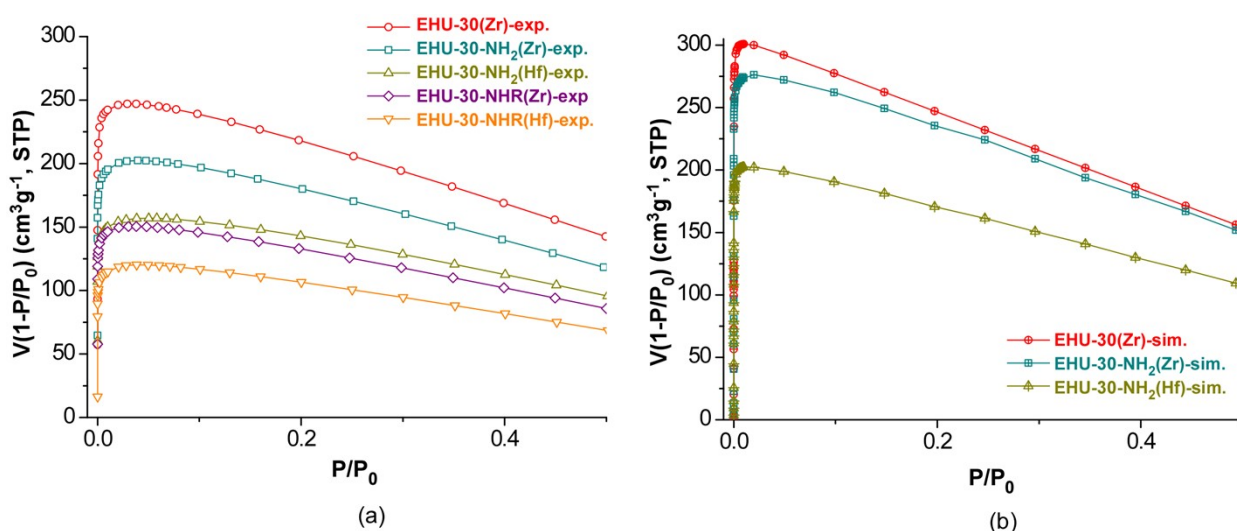


Figure S9.2. Consistency plot [$V(1 - P/P_0)$ vs. P/P_0] for experimental and simulated N_2 isotherms.

Table S9.1. BET fitting details for experimental and simulated N_2 isotherms.

Code	P/P_0 range	S_{BET} (m^2/g)	R^2	C	V_m (cm^3/g)	P/P_0 for V_m (interpolation)
EHU-30-NH ₂ (Zr) Experimental	0.0041 – 0.0396	891	0.99999	2374.7	204.51	0.02064
EHU-30-NH ₂ (Hf) Experimental	0.0060 – 0.0503	691	0.99999	1837.7	158.63	0.02280
EHU-30-NHR(Zr) Experimental	0.0040 – 0.0381	662	0.99999	2921.5	151.91	0.01819
EHU-30-NHR(Hf) Experimental	0.0061 – 0.0384	531	0.99999	1738.7	121.93	0.02343
EHU-30(Zr) Experimental	0.0020 – 0.0294	1083	0.99999	4288.2	248.78	0.01505

²⁰ D. A. Gómez-Gualdrón, P. Z. Moghadam, J. T. Hupp, O. K. Farha and R. Q. Snurr, Application of Consistency Criteria To Calculate BET Areas of Micro- And Mesoporous Metal–Organic Frameworks, *J. Am. Chem. Soc.*, 2016, **138**, 215–224. <https://doi.org/10.1021/jacs.5b10266>

²¹ (a) O. K. Farha, A. O. Yazaydin, I. Eryazici, C. D. Malliakas, B. G. Hauser, M. G. Kanatzidis, S. T. Nguyen, R. Q. Snurr and J. T. Hupp, De novo synthesis of a metal–organic framework material featuring ultrahigh surface area and gas storage capacities, *Nat. Chem.*, 2010, **2**, 944–948. <https://doi.org/10.1038/nchem.834>, (b) H. Furukawa, N. Ko, Y. B. Go, N. Aratani, S. B. Choi, E. Choi, A. O. Yazaydin, R. Q. Snurr, M. O’Keeffe, J. Kim and O. M. Yaghi, . Ultrahigh Porosity in Metal–Organic Frameworks, *Science*, 2010, **329**, 424–428. <https://doi.org/10.1126/science.1192160>, (c) O. K. Farha, I. Eryazici, N. C. Jeong, B. G. Hauser, C. E. Wilmer, A. A. Sarjeant, R. Q. Snurr, S. T. Nguyen, A. O. Yazaydin and J. T. Hupp, Metal–Organic Framework Materials with Ultrahigh Surface Areas: Is the Sky the Limit?, *J. Am. Chem. Soc.*, 2012, **134**, 15016–15021. <https://doi.org/10.1021/ja3055639>, (d) O. K. Farha, I. Eryazici, N. C. Jeong, B. G. Hauser, C. E. Wilmer, A. A. Sarjeant, R. Q. Snurr, S. T. Nguyen, A. O. Yazaydin and J. T. Hupp, Applicability of the BET Method for Determining Surface Areas of Microporous Metal–Organic Frameworks, *J. Am. Chem. Soc.*, 2012, **134**, 8552–8556. <https://doi.org/10.1021/ja071174k>

EHU-30(Zr) Simulated	0.0009 – 0.0099	1320	0.99999	14810.0	303.07	0.00815
EHU-30-NH₂(Zr) Simulated	0.0010 – 0.0099	1204	0.9999	10226.18	276.34	0.00979
EHU-30-NH₂(Hf) Simulated	0.0010 – 0.0099	888	0.99999	13879.4	202.8	0.00841

CO₂ adsorption isotherms and calculation of isosteric heats of adsorption

Figure S9.3 represents experimental CO₂ adsorption isotherms measured at 298 K for EHU-30(Zr), EHU-30-NH₂(Zr and Hf-based) and for EHU-30-NHR(Zr and Hf-based) samples. In order to estimate CO₂ adsorption enthalpies (Q_{st}), the isotherms were fitted to modified Clausius–Clapeyron equation.²² Resulting data are gathered in Figure S9.4. Finally, Figure S9.5 represents simulated CO₂ isotherm measured at 273 K of EHU-30, EHU-30-NH₂(Zr) and EHU-30-NH₂(Hf).

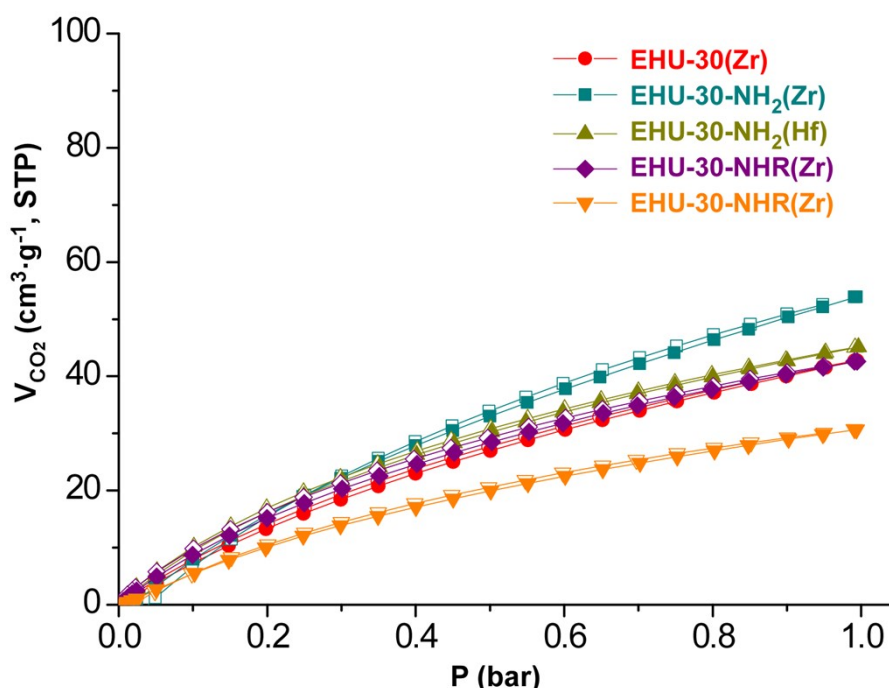


Figure S9.3. Experimental CO₂ adsorption isotherms at 298 K measured upon EHU-30, EHU-30-NH₂ and EHU-30-NHR samples. Samples. Closed symbols, adsorption; open symbols, desorption.

²² (a) K. Sumida, D. L. Rogow, J. A. Mason, T. M. McDonald, E. D. Bloch, Z. R. Herm, T-H. Bae and J. R. Long, Carbon Dioxide Capture in Metal–Organic Frameworks, *Chem. Rev.*, 2012, **112**, 724–781. <https://doi.org/10.1021/cr2003272>; (b) H. Pan, J. A. Ritter and P. B. Balbuena, Examination of the Approximations Used in Determining the Isosteric Heat of Adsorption from the Clausius–Clapeyron Equation, *Langmuir*, 1998, **14**, 6323–6327. <https://doi.org/10.1021/la9803373>

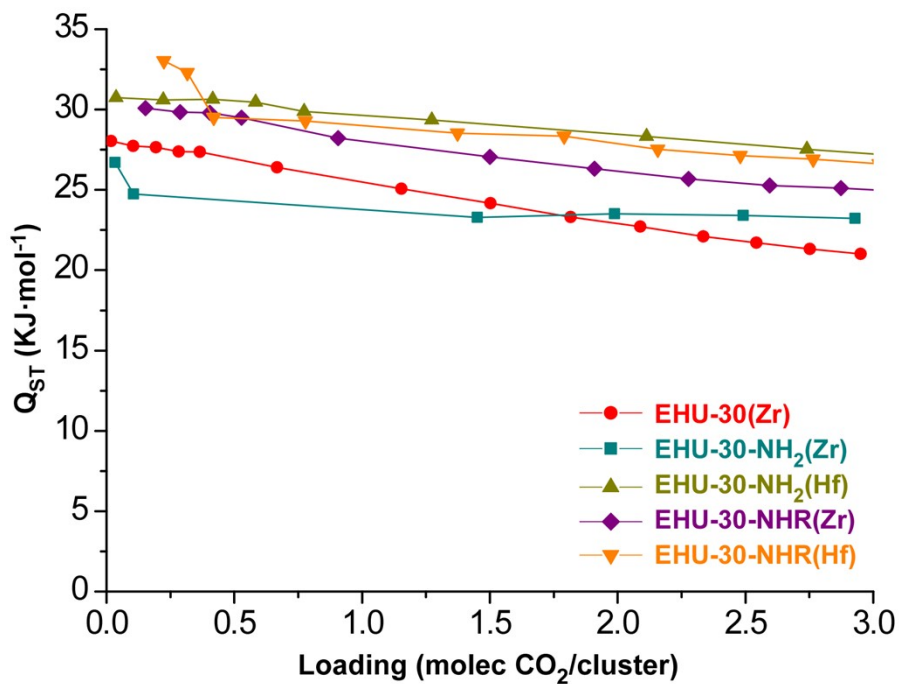


Figure S9.4. Calculated isosteric heats of adsorption for CO₂.

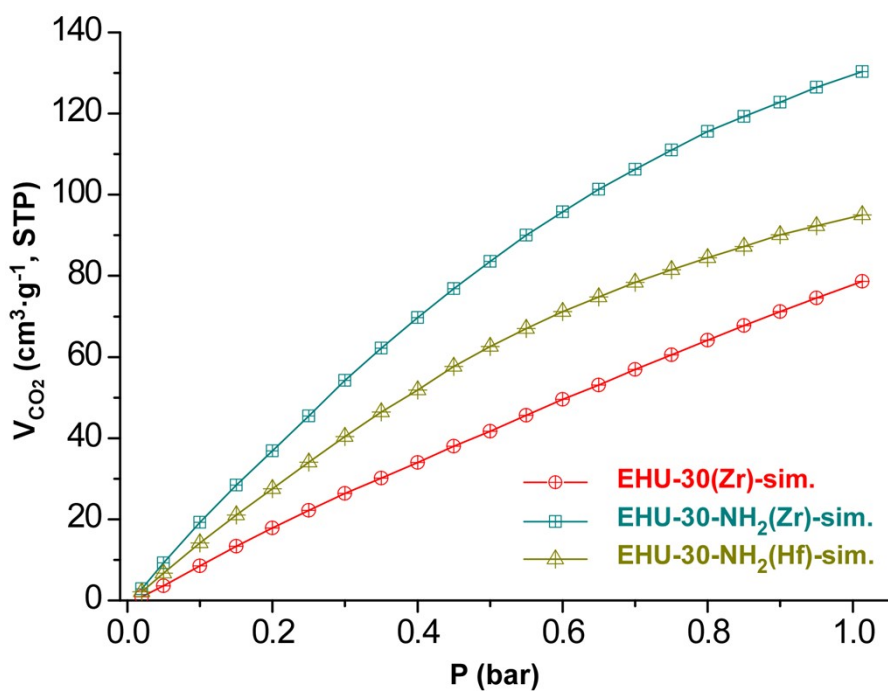


Figure S9.5. Simulated CO₂ adsorption isotherms at 273 K measured upon EHU-30(Zr), EHU-30-NH₂(Zr) and EHU-30-NHR(Zr) samples.

S10. WATER-VAPOUR ADSORPTION OF EHU-30(Zr), EHU-30-NH₂(Zr) AND EHU-30-NHR(Zr)

Experimental water-vapour isotherms

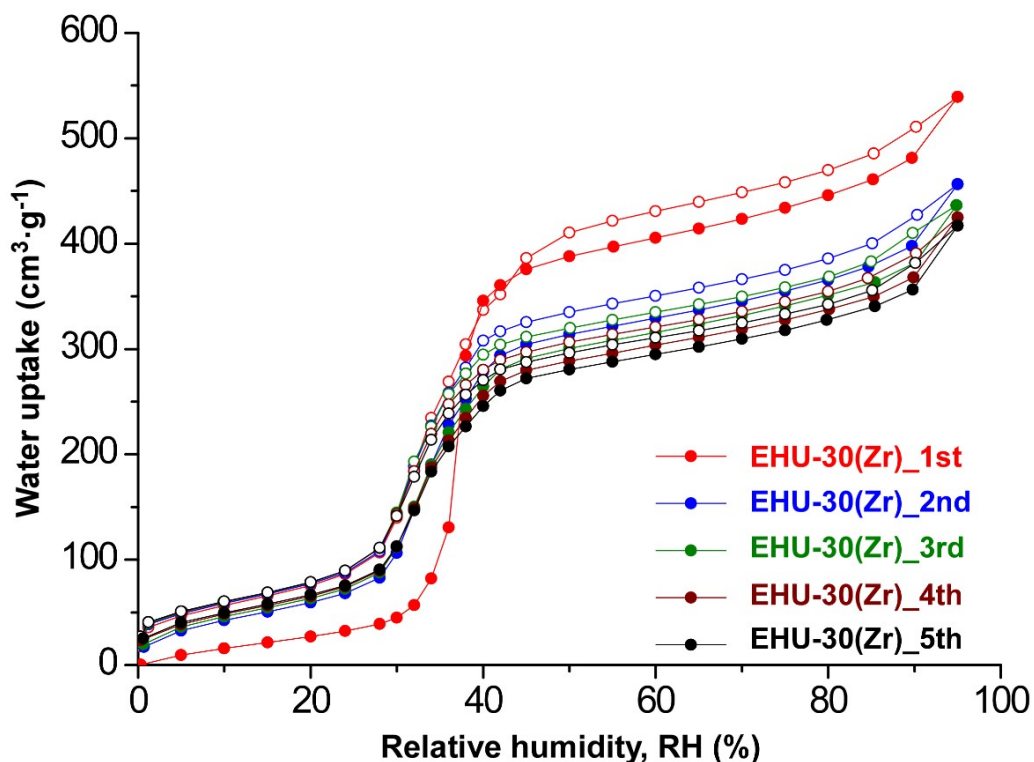


Figure S10.1. Cyclability of water vapour adsorption of EHU-30(Zr) measured at 25°C. Closed symbols, adsorption; open symbols, desorption.

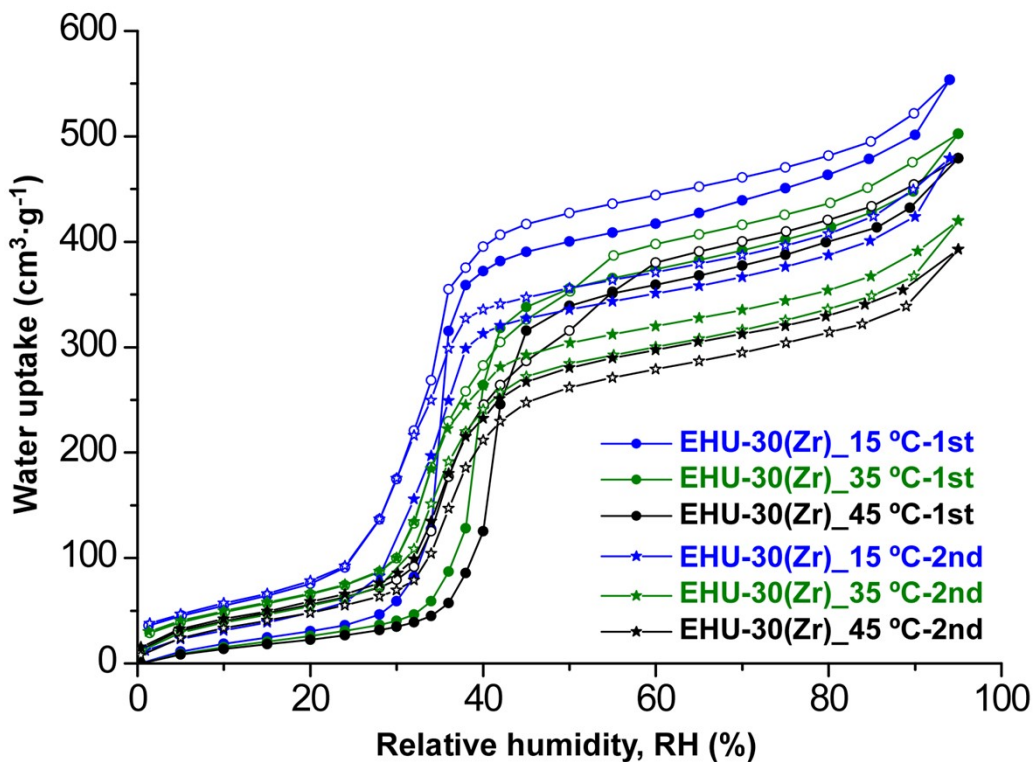


Figure S10.2. First and second cycle of water vapour adsorption of EHU-30 measured at 15°C, 35°C and 45°C. Closed symbols, adsorption; open symbols, desorption.

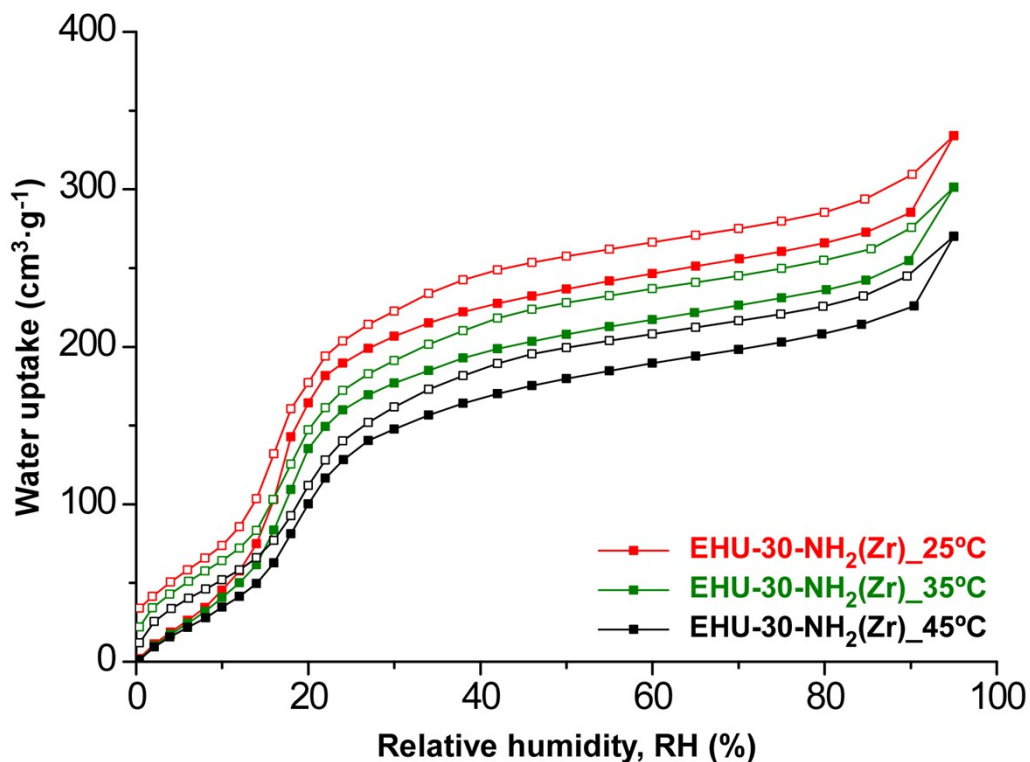


Figure S10.3. Water vapour adsorption isotherms of EHU-30-NH₂(Zr) measured at 25°C, 35°C and 45°C. Closed symbols, adsorption; open symbols, desorption.

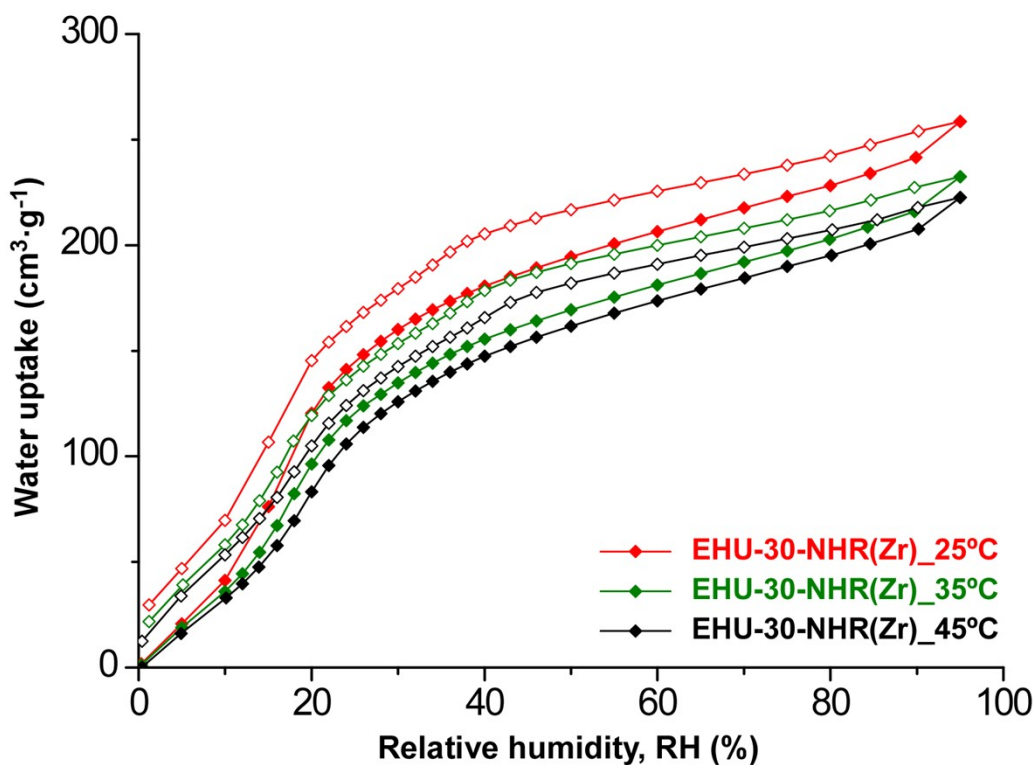


Figure S10.4. Water vapour adsorption isotherms of EHU-30-NHR(Zr) measured at 25°C, 35°C and 45°C. Closed symbols, adsorption; open symbols, desorption.

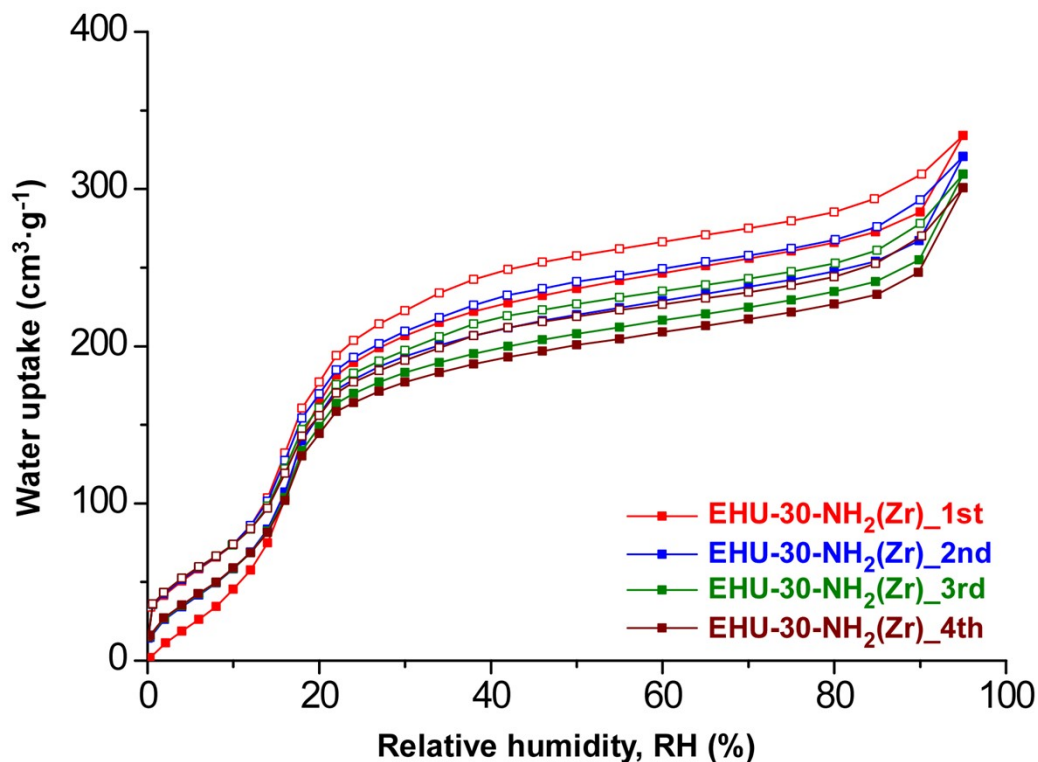


Figure S10.5. Cyclability of water vapour adsorption of EHU-30-NH₂(Zr) measured at 25°C. Closed symbols, adsorption; open symbols, desorption.

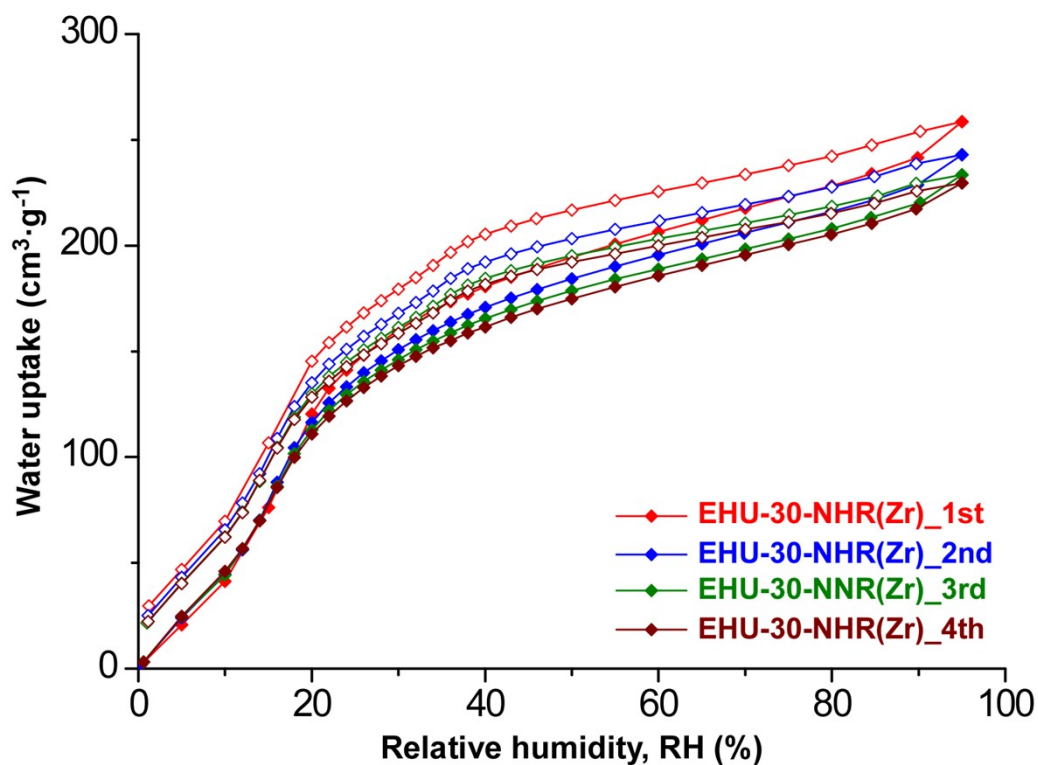


Figure S10.6. Cyclability of water vapour adsorption of EHU-30-NHR(Zr) measured at 25°C. Closed symbols, adsorption; open symbols, desorption.

Simulated water-vapour isotherms

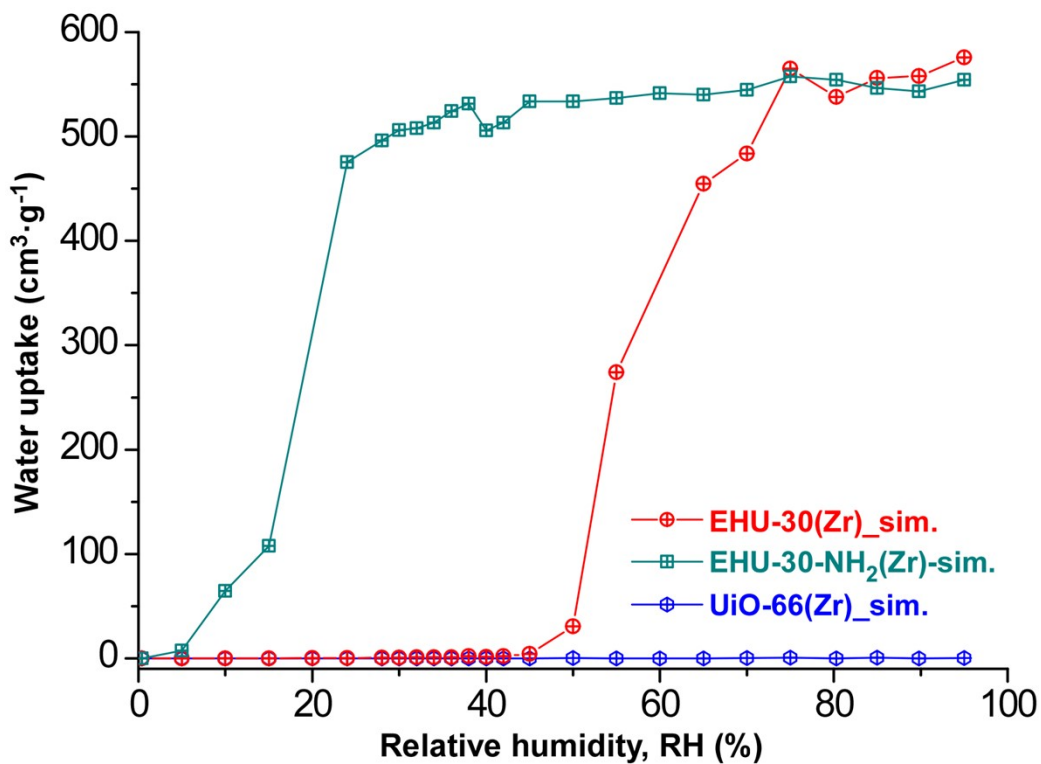


Figure S10.7. Simulated water vapour adsorption isotherms of EHU-30(Zr), EHU-30-NH₂(Zr) and UiO-66(Zr) measured at 25°C.

PXRD patterns before and after the water vapour adsorption

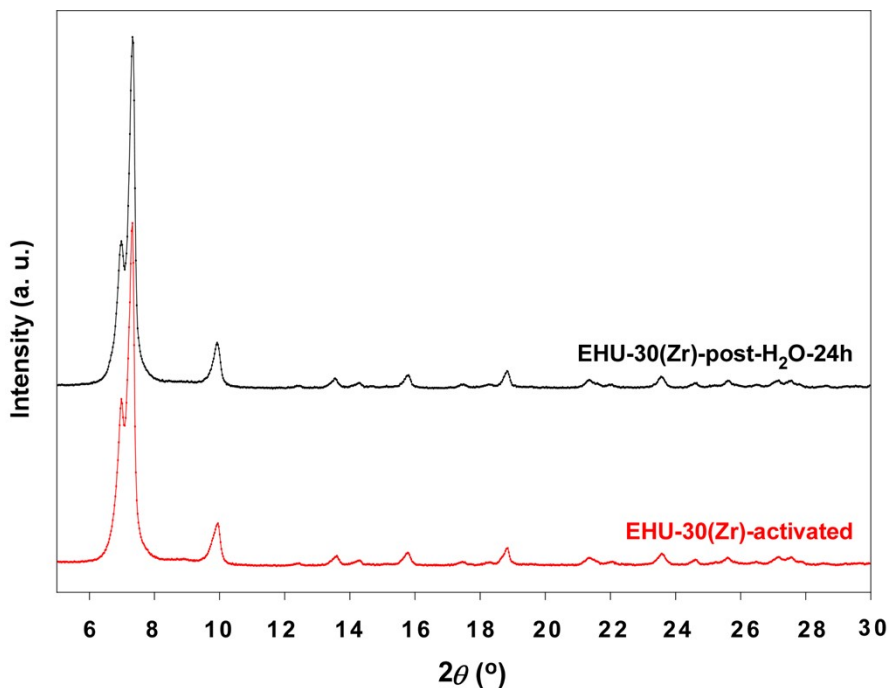


Figure S10.8. PXRD patterns of EHU-30(Zr) before and after exposure to liquid water during 24h.

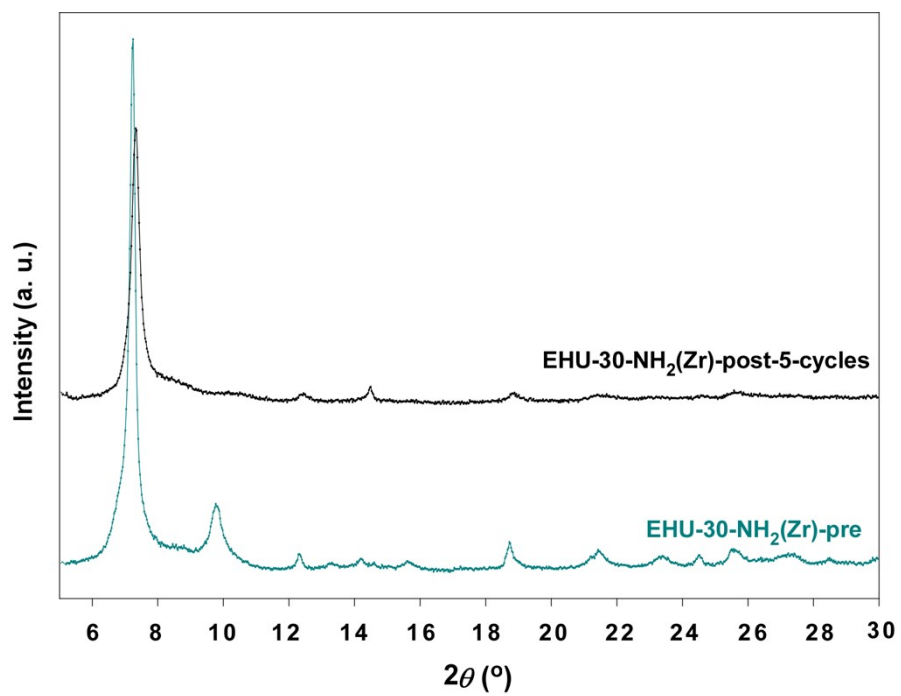


Figure S10.9. PXRD patterns of EHU-30-NH₂(Zr) before and after exposure to 5 cycles of water vapour adsorption at 25 °C.

S11. LOCATION OF WATER MOLECULES BY TOF NEUTRON POWDER DIFFRACTION

S11. LOCATION OF WATER MOLECULES BY TOF NEUTRON POWDER DIFFRACTION

TOF powder neutron diffraction patterns of polycrystalline EHU-30(Zr), D₂O@EHU-30(Zr), EHU-30-NH₂(Zr), and D₂O@EHU-30-NH₂(Zr) were measured on GEM diffractometer at the ISIS Neutron and Muon Source, UK. Samples were mounted on 6 mm-diameter cylindrical vanadium sample holders and data was collected at 293 K.

Crystal structures of all four samples were refined using Topas Academic v6 program. For the case of water loaded samples, the preferred adsorption sites for D₂O molecules were revealed by means of subsequent difference Fourier map calculations and Rietveld refinements where the framework atomic positions were kept fixed. The final Rietveld refinements included the atomic coordinates of all atoms and GEM detectors banks 1 to 4, simultaneously. For each refinement, an isotropic atomic displacement parameter was applied for the metal atom, while an overall parameter was introduced for the light atoms, and H/D occupancies were refined for the hydrogen crystallographic sites on the frameworks. On the final fits, there were 93, 127, 95 and 111 different adjustable parameters, respectively (scale factor, background, unit-cell parameters, peak-shape parameters, atomic coordinates, and temperature factors). Figures S11.1 to S11.4 show the final Rietveld fits for EHU-30(Zr), D₂O@EHU-30(Zr), EHU-30-NH₂(Zr), and D₂O@EHU-30-NH₂(Zr), respectively. Table S11.1 summarizes the corresponding crystallographic and refinement-related data, while obtained final atomic coordinates are reported in Tables S11.2 to S11.5.

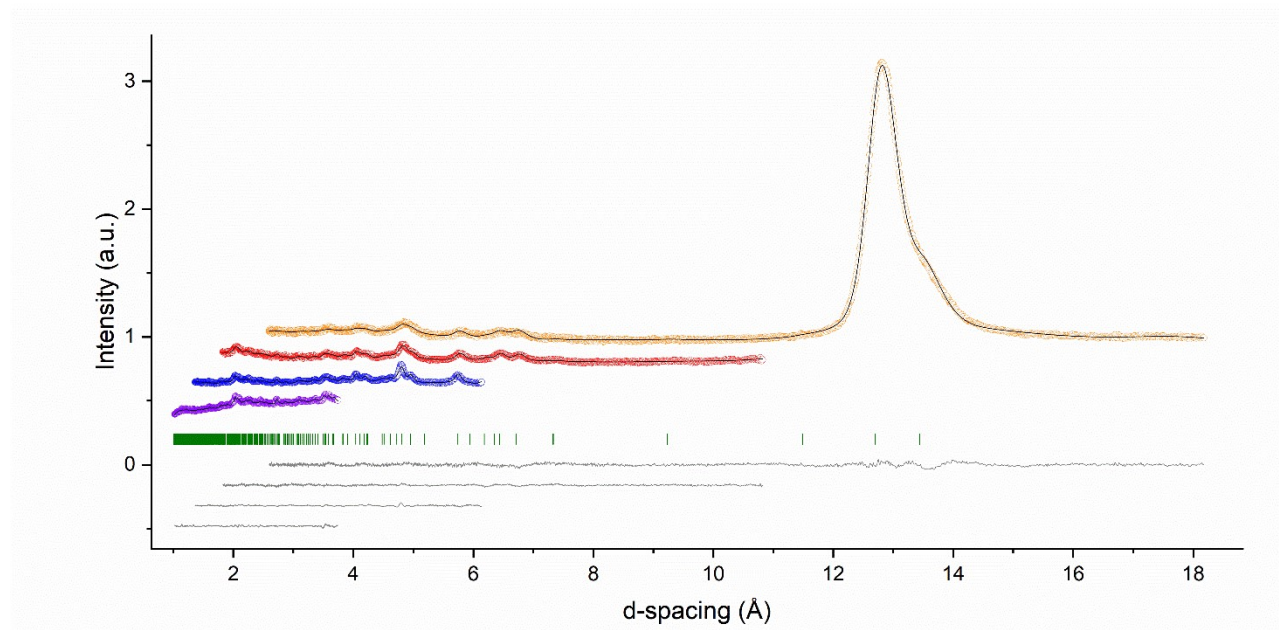


Figure S11.1. Final Rietveld refinement plot for EHU-30(Zr), showing the experimental (open circles) profiles for banks 1, 2, 3 and 4 (orange, red, blue and violet, respectively). Calculated and difference profiles are shown as black and grey lines, respectively, while green tick marks indicate reflection positions.

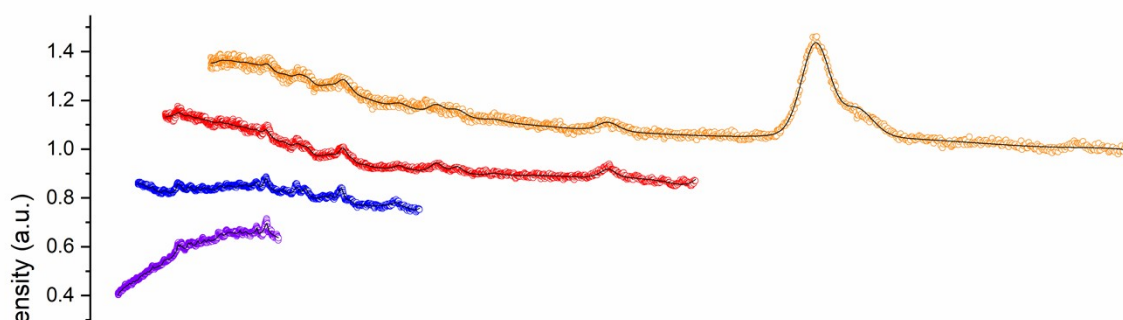


Figure S11.2. Final Rietveld refinement plot for $D_2O@EHU-30(Zr)$, showing the experimental (open circles) profiles for banks 1, 2, 3 and 4 (orange, red, blue and violet, respectively). Calculated and difference profiles are shown as black and grey lines, respectively, while green tick marks indicate reflection positions.

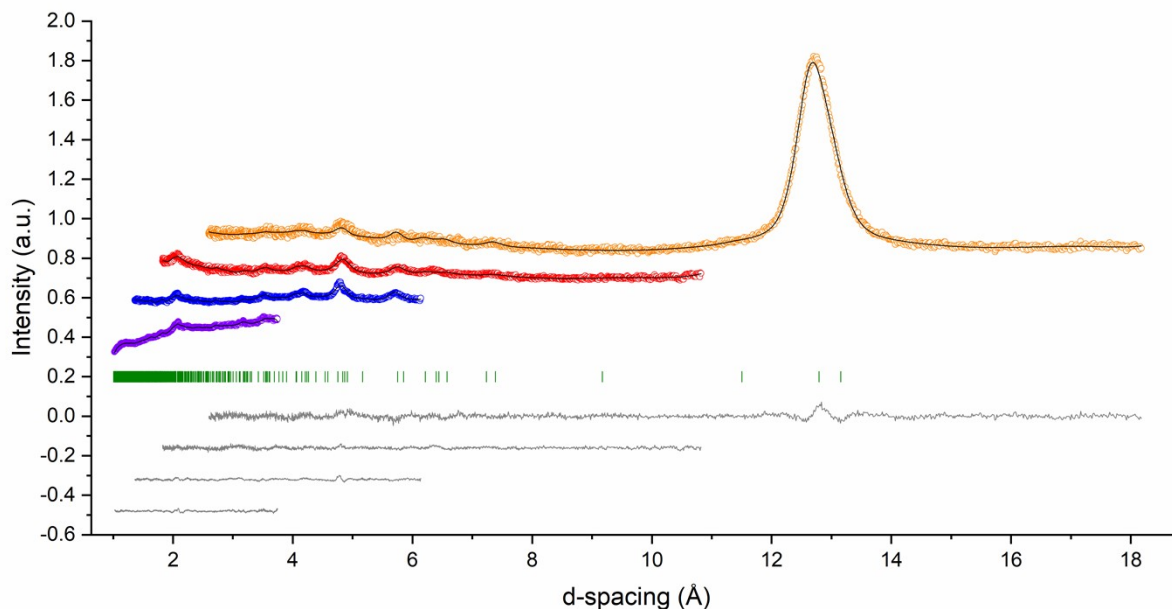


Figure S11.3. Final Rietveld refinement plot for $EHU-30-NH_2(Zr)$, showing the experimental (open circles) profiles for banks 1, 2, 3 and 4 (orange, red, blue and violet, respectively). Calculated and difference profiles are shown as black and grey lines, respectively, while green tick marks indicate reflection positions.

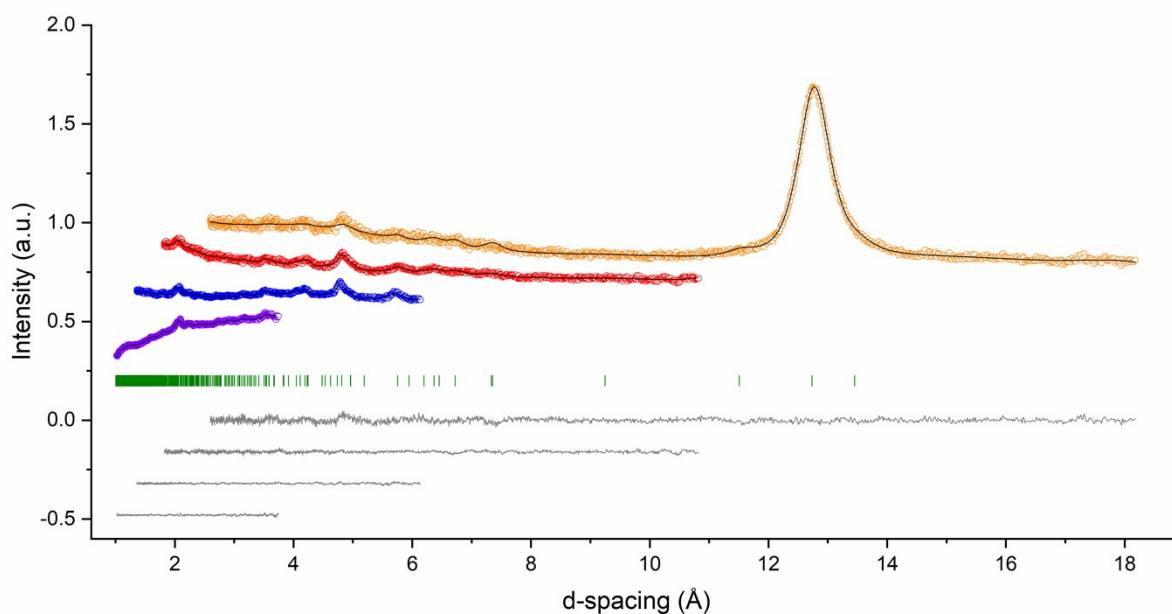


Figure S11.4. Final Rietveld refinement plot for $D_2O@EHU-30-NH_2(Zr)$, showing the experimental (open circles) profiles for banks 1, 2, 3 and 4 (orange, red, blue and violet, respectively). Calculated and difference

profiles are shown as black and grey lines, respectively, while green tick marks indicate reflection positions.

Table S11.1. Crystallographic data and Rietveld refinement summary for EHU-30(Zr), D₂O@EHU-30(Zr), EHU-30-NH₂(Zr) and D₂O@EHU-30-NH₂(Zr).

Compound	EHU-30(Zr)	D ₂ O@EHU-30(Zr)	EHU-30-NH ₂ (Zr)	D ₂ O@EHU-30-NH ₂ (Zr)
Formula	Zr ₆ (C ₈ H ₃ D ₁ O ₄) ₆ O ₈	Zr ₆ (C ₈ H _{0.54} D _{3.46} O ₄) ₆ O ₈ ·(D ₂ O) _{7.98}	Zr ₆ (C ₈ H _{4.18} D _{0.82} NO ₄) ₆ O ₈	Zr ₆ (C ₈ H _{1.28} D _{3.72} O ₄) ₆ O ₈ ·(D ₂ O) _{6.94}
Formula weight (g/mol)	1664.979	1840.737	1765.434	1911.485
<i>D_c</i> (g/cm ³)	1.10069	1.18231	1.16906	1.23250
Crystal system	Hexagonal	Hexagonal	Hexagonal	Hexagonal
Space group	<i>P6₃/mmc</i>	<i>P6₃/mmc</i>	<i>P6₃/mmc</i>	<i>P6₃/mmc</i>
<i>a</i> (Å)	14.669(4)	14.733(10)	14.772(14)	14.706(11)
<i>c</i> (Å)	26.879(8)	26.949(17)	26.31(3)	26.88(2)
<i>V</i> (Å ³)	5009(3)	5066(7)	4972(11)	5034(9)
<i>Z</i>	2	2	2	2
Radiation type	Neutrons	Neutrons	Neutrons	Neutrons
Diffractionmeter	GEM, ISIS Facility	GEM, ISIS Facility	GEM, ISIS Facility	GEM, ISIS Facility
Data collection mode	Time-of-flight	Time-of-flight	Time-of-flight	Time-of-flight
<i>R_p</i> (%)	0.88	0.49	0.75	0.52
<i>R_{wp}</i> (%)	0.85	0.45	0.67	0.41
<i>R_{exp}</i> (%)	0.50	0.35	0.50	0.04
<i>R_B</i> (%)	0.23	0.18	0.48	0.07
Goodness-of-fit	1.70	1.29	1.34	1.03

Table S11.2. Fractional atomic coordinates and isotropic displacement parameter (Å²) of non-H atoms for EHU-30(Zr).

Atom	<i>x</i>	<i>y</i>	<i>z</i>	<i>B_{iso}</i>	Occupancy
Zr1	0.8386(13)	-0.0807(7)	0.0476(5)	7.2(6)	1
O1	0.8241(9)	-0.0880(4)	-0.0319(4)	0.5(4)	1
O2	1	0	0.0738(9)	0.5(4)	1
C1_1	0.5112(3)	-0.07200(19)	0.02999261	12.2(5)	1
H1_1	0.5199(5)	-0.1279(3)	0.0532609	14.6(6)	0.984(10)
D1_1	0.5199(5)	-0.1279(3)	0.0532609	14.6(6)	0.016(10)
C3_1b	0.59584(18)	0	0	12.2(5)	1
C4_1b	0.6782(3)	0	0	12.2(5)	1
O5_1	0.6924(13)	-0.0608(10)	0.02730(19)	12.2(5)	1
C1_2	0.8079(11)	-0.221(2)	0.22431(15)	12.2(5)	1
H1_2	0.7507(18)	-0.208(3)	0.2045(3)	14.6(6)	0.516(10)
D1_2	0.7507(18)	-0.208(3)	0.2045(3)	14.6(6)	0.484(10)

C3_2b	0.8893(10)	-0.221(2)	0.198598(3)	12.2(5)	1
C4_2b	0.8986(14)	-0.203(3)	0.14461(6)	12.2(5)	1
O5_2	0.843(2)	-0.176(3)	0.1208(7)	12.2(5)	1

Table S11.3. Fractional atomic coordinates and isotropic displacement parameter (\AA^2) of non-H atoms for $\text{D}_2\text{O@EHU-30}(\text{Zr})$.

Atom	x	y	z	B_{iso}	Occupancy
Zr1	0.839(3)	-0.0805(17)	0.0516(15)	4.8(9)	1
O1	0.837(2)	-0.0813(11)	-0.0282(13)	0.5(8)	1
O2	1	0	0.075(3)	0.5(8)	1
C1_1	0.5318(6)	-0.0315(12)	0.0427(2)	5.0(5)	1
H1_1	0.5564(11)	-0.056(2)	0.0758(4)	6.0(6)	0.24(2)
D1_1	0.5564(11)	-0.056(2)	0.0758(4)	6.0(6)	0.76(2)
C3_1b	0.5953(5)	0	0	5.0(5)	1
C4_1b	0.6937(10)	0	0	5.0(5)	1
O5_1	0.720(2)	-0.029(2)	0.0389(5)	5.0(5)	1
C1_2	0.819(2)	-0.199(4)	0.2243(3)	5.0(5)	1
H1_2	0.762(3)	-0.186(6)	0.2046(5)	6.0(6)	0.03(2)
D1_2	0.762(3)	-0.186(6)	0.2046(5)	6.0(6)	0.97(2)
C3_2b	0.900(2)	-0.199(4)	0.198606(7)	5.0(5)	1
C4_2b	0.910(3)	-0.181(6)	0.14540(14)	5.0(5)	1
O5_2	0.852(4)	-0.155(5)	0.1248(14)	5.0(5)	1
O1_w1	0.212(3)	0.788(3)	0.491(3)	1.0(19)	0.46(2)
D1_w1	0.243(13)	0.847(7)	0.469(5)	1.0(19)	0.231(12)
D2_w1	0.137(4)	0.750(12)	0.488(7)	1.0(19)	0.231(12)
O1_w2	-0.022(6)	0.489(3)	0.849(2)	1.0(13)	0.57(3)
D1_w2	-0.01(5)	0.554(18)	0.862(11)	1.0(13)	0.286(14)
D2_w2	0.013(11)	0.50(2)	0.817(3)	1.0(13)	0.286(14)
O1_w3	$\frac{2}{3}$	$\frac{1}{3}$	0.0568(19)	1(2)	0.30(2)
D1_w3	0.61(5)	0.29(3)	0.08(2)	1(2)	0.101(7)
D2_w3	0.72(3)	0.396(16)	0.075(17)	1(2)	0.101(7)

Table S11.4. Fractional atomic coordinates and isotropic displacement parameter (\AA^2) of non-H atoms for $\text{EHU-30-NH}_2(\text{Zr})$.

Atom	x	y	z	B_{iso}	Occupancy
Zr1	0.840(4)	-0.0799(18)	0.050(2)	15(2)	1
O1	0.8312(17)	-0.0844(9)	-0.0313(16)	0.5(7)	1
O2	1	0	0.0755(17)	0.5(7)	1
C1_1	0.5411(13)	-0.013(3)	0.04587(17)	15.4(12)	1
H1_1	0.573(2)	-0.023(5)	0.0815(3)	18.4(14)	0.75(4)
D1_1	0.573(2)	-0.023(5)	0.0815(3)	18.4(14)	0.00(4)
N1_1	0.582(5)	-0.025(5)	0.091(4)	18.4(14)	0.25
H5_1a	0.540(5)	-0.035(8)	0.127(4)	18.4(14)	0.16(3)
H5_1b	0.655(5)	-0.025(6)	0.091(4)	18.4(14)	0.16(3)

D5_1a	0.540(5)	-0.035(8)	0.127(4)	18.4(14)	0.09(3)
D5_1b	0.655(5)	-0.025(6)	0.091(4)	18.4(14)	0.09(3)
C3_1b	0.5951(7)	0	0	15.4(12)	1
C4_1b	0.6838(14)	0	0	15.4(12)	1
O5_1	0.724(3)	-0.011(4)	0.0396(7)	15.4(12)	1
C1_2	0.796(3)	-0.247(5)	0.2237(4)	15.4(12)	1
H1_2	0.739(4)	-0.234(7)	0.2035(7)	18.4(14)	0.75(7)
D1_2	0.739(4)	-0.234(7)	0.2035(7)	18.4(14)	0.00(7)
N1_2	0.722(12)	-0.230(8)	0.198(4)	18.4(14)	0.25
H5_2a	0.729(12)	-0.217(8)	0.157(4)	18.4(14)	0.13(4)
H5_2b	0.658(13)	-0.230(10)	0.218(4)	18.4(14)	0.13(4)
D5_2a	0.729(12)	-0.217(8)	0.157(4)	18.4(14)	0.12(4)
D5_2b	0.658(13)	-0.230(10)	0.218(4)	18.4(14)	0.12(4)
C3_2b	0.877(3)	-0.247(5)	0.197358(11)	15.4(12)	1
C4_2b	0.886(4)	-0.228(8)	0.1421(2)	15.4(12)	1
O5_2	0.832(5)	-0.201(8)	0.118(2)	15.4(12)	1

Table S11.5. Fractional atomic coordinates and isotropic displacement parameter (\AA^2) of non-H atoms for $\text{D}_2\text{O@EHU-30-NH}_2(\text{Zr})$.

Atom	x	y	z	B_{iso}	Occupancy
Zr1	0.842(2)	-0.0790(12)	0.0420(14)	11.0(13)	1
O1	0.8138(13)	-0.0931(7)	-0.0308(9)	1.0(5)	1
O2	1	0	0.0741(14)	1.0(5)	1
C1_1	0.5316(10)	-0.0321(17)	0.0427(3)	23.6(11)	1
H1_1	0.5561(17)	-0.057(3)	0.0758(6)	28.3(13)	0.00(4)
D1_1	0.5561(17)	-0.057(3)	0.0758(6)	28.3(13)	0.75(4)
N1_1	0.563(5)	-0.064(6)	0.085(6)	28.3(13)	0.25
H5_1a	0.513(5)	-0.089(7)	0.118(6)	28.3(13)	0.15(3)
H5_1b	0.637(5)	-0.064(6)	0.085(6)	28.3(13)	0.15(3)
D5_1a	0.513(5)	-0.089(7)	0.118(6)	28.3(13)	0.10(3)
D5_1b	0.637(5)	-0.064(6)	0.085(6)	28.3(13)	0.10(3)
C3_1	0.5955(11)	0	0	23.6(11)	1
C4_1	0.689(2)	0	0	23.6(11)	1
O5_1	0.716(4)	-0.029(4)	0.0388(7)	23.6(11)	1
C1_2	0.803(2)	-0.228(4)	0.2239(4)	23.6(11)	1
H1_2	0.746(3)	-0.215(6)	0.2041(6)	28.3(13)	0.24(6)
D1_2	0.746(3)	-0.215(6)	0.2041(6)	28.3(13)	0.51(6)
N1_2	0.730(9)	-0.211(6)	0.198(3)	28.3(13)	0.25
H5_2a	0.737(9)	-0.198(7)	0.158(3)	28.3(13)	0.05(3)
H5_2b	0.665(9)	-0.211(8)	0.219(3)	28.3(13)	0.05(3)
D5_2a	0.737(9)	-0.198(7)	0.158(3)	28.3(13)	0.20(3)
D5_2b	0.665(9)	-0.211(8)	0.219(3)	28.3(13)	0.20(3)
C3_2	0.886(2)	-0.228(5)	0.197723(8)	23.6(11)	1
C4_2	0.896(3)	-0.209(7)	0.14364(16)	23.6(11)	1
O5_2	0.841(5)	-0.182(6)	0.1202(18)	23.6(11)	1

O1_w1	0.31(3)	0.707(19)	0.313(4)	9(3)	0.191(8)
D1_w1	0.29(4)	0.74(4)	0.288(5)	9(3)	0.191(8)
D2_w1	0.32(4)	0.74(3)	0.345(6)	9(3)	0.191(8)
O1_w2	0.940(4)	0.547(4)	0.2192(14)	5.0(11)	0.387(12)
D1_w2	0.966(17)	0.512(15)	0.1976(18)	5.0(11)	0.387(12)
D2_w2	0.948(8)	0.532(9)	0.2536(15)	5.0(11)	0.387(12)